5

L-TYROSINE BASED CHIRAL POLY (ESTER-AMIDE) S CONTAINING MAIN CHAIN AND SIDE CHAIN AZO GROUP

5.1. Introduction

Amino acids and amino acid derivatives have been demonstrated to function as highly useful chiral auxiliaries for a variety of nitro aromatics and other D-A molecules with large hyperpolarizabilities.[1] Phasematching L-arginine phosphate crystals generates second harmonic signals greater than that of quartz.[2] Solid state structures of some urea-based peptidomimetics containing β-alanyl unit have shown self-assembly into highly ordered, extended hydrogen-bonded chains and ribbons with modest NLO activity.[3] In addition to this function, these molecules are in their own right also of potential for second harmonic generation. Harmonic generation efficiency of single crystals of L-alanine,[4] and L-threonine [5] are well studied. Simple derivatives of amino acids have not been adequately examined, and many substances potentially useful for harmonic generation into the UV remain to be found. For example, among the derivatives of amino acids, N-acetyl cystein is highly crystalline, damage resistant, and has a powder efficiency about one-third that of urea.[1] L-tyrosine is an unexplored amino acid in the field of NLO studies. Present study has been focused on the molecular design of highly efficient chiral chromophore based on L-tyrosine.

In general, aromatic ring containing polyamide matrices, which are easily prepared from the corresponding carboxylic acid/anhydride functionalized monomers and the amino-functionalized ones, exhibit relatively high *Tg*'s. Indeed, the preparation of second-order NLO active main-chain and side-chain type polyamides has been reported. [6] In our laboratory, poly (ester amide) s based on bismaleamic acid have been investigated as good SHG material.[7] The primary interest of this study is to design and investigate the NLO properties of L-tyrosine based chiral poly (ester-amide) s

incorporated with different chiral and achiral moieties which increases the NLO response and also with high polymer stability by contributing high Tg values to the polymer.[8]

This chapter includes the design of L-tyrosine based chromophore with high β values. It also includes the design of chiral and achiral diols for polycondensation with the designed chromophore for the purpose of studying the effect of incorporation of additional chiral molecules into an already chiral medium. The synthesis was done after the design of the molecules and theoretical evaluations of the NLO properties was performed. Thus, the *state-of-art* of design and synthesis of highly active NLO materials have been followed in this study.

5.2. Computational methods

5.2.1. Monomers

Since L-tyrosine based chromophores contain more than 400 electrons, geometry optimizations including the polarized and diffused basis sets even with density functional methods are computationally highly demanding. Hence, all the monomers have been optimized to Hartree-Fock common level of theory to avoid the geometry effects in the prediction because of high sensitivity of polarizability to geometry. All the L-tyrosine based chromophores and diol monomers have been optimized with 6-31G basis sets using restricted Hartree-Fock formalism available with the Gaussian algorithm.[9] The optimized geometries were used to compute the SCF MO energies. The *static* spectroscopic properties of monomers have been calculated using Coupled Perturbed Hartree-Fock (CPHF) method at RHF 6-31++G(d,p) level available in the Gaussian codes.[10] The *dynamic* spectroscopic properties have been calculated using the Zerner's INDO-SOS method with sum over 82 states.[11]

5.2.2. Polymers

All the polymer geometries (three repeating units) have been optimized using the AM1 parameterized Hamiltonian available in the Gaussian 03 set of codes.[12] The

geometries obtained by AM1 calculations have been compared with geometries obtained using *ab initio* methods at 6-31G level for polymers. Both the geometries have comparable bond lengths and bond angles. Compared to the small difference in bond length and bond angle, the computational demand for *ab initio* method is much more for polymers. Hence, geometry calculations are restricted to this semi-empirical level. Also, because of the very high cost of computation in calculating the properties of polymers (repeating units) using polarized and diffused basis sets, *static* (CPHF) molecular properties of polymers have been limited with 6-31 G(d) basis sets. The *dynamic* spectroscopic properties have been calculated using the Zerner's INDO-SOS method with sum over 82 states.

5.3. Designing of molecules

In this chapter, the main concentration was on the chromophore design based on L-tyrosine. Since L-tyrosine is a potential chiral auxiliary for NLO material, the goal has been targeted to the addition of nitroaromatics and donor-acceptor groups (e.g. *para*-nitroaniline, azo-acid chloride) into the L-tyrosine framework. The diols have been selected on the basis of the coupling ability with the L-tyrosine framework to form polymers with high β value. Both chiral and achiral diols have been selected so as to study the effect on the β value by the incorporation of chiral and achiral molecules in to a chiral medium

5.3.1. Monomer design

5.3.1.1 Chromophore

The route of chromophore design is shown in **Figure 5.1.** The basic chemistry, of organic donor- acceptor NLO materials has been developed on the basis of *para*-nitroaniline (**1**) In this design, *para*-nitroaniline (PNA) was diazotized and coupled with the amino acid, L-tyrosine (Tyr, **2**), to provide the basic chiral framework of (*S*)-2-amino-3-(3-(4-nitrophenylazo)-4-hydroxyphenyl) propanoic acid (PNATY, **3**). By the acylation of PNATY with azobenzene-4, 4'-dicarbonyl chloride (AZCl, **4**), chiral amide framework, bis{(S)-2-(4-azenyl benzamido)-3-(3-(4-nitrophenylazo)-4-hydroxyphenyl) propanoic

acid (TYAZ, 5) was designed. Chlorination of TYAZ yielded the bis[(S)-2-(4-azenyl benzamido)-3-(3-(4-nitrophenylazo)- 4-hydroxyphenyl) propanoic acidchloride (TYAZCl,6).

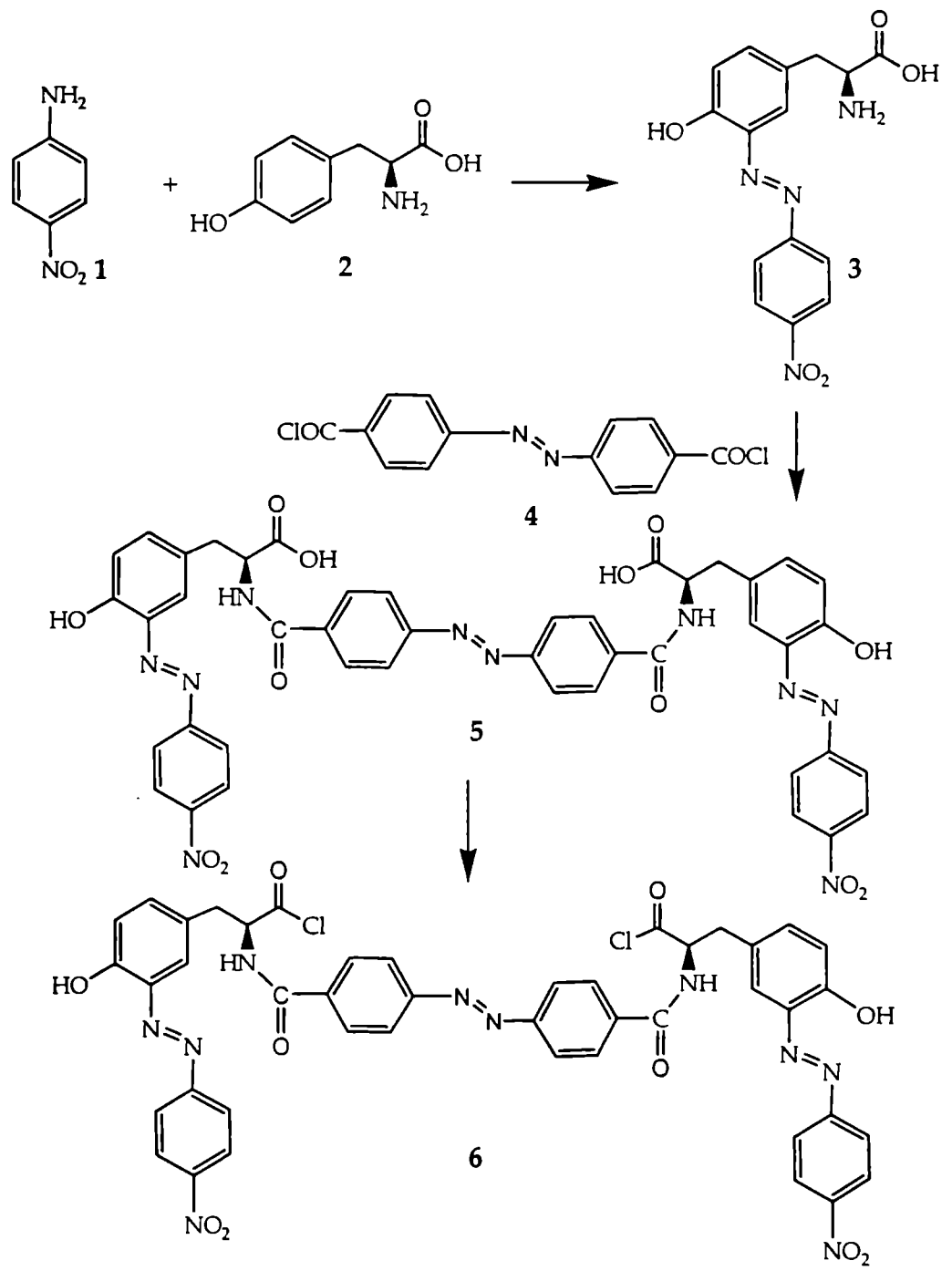

Figure 5.1. Route of chromophore design

5.3.1.1.1. Static and Dynamic molecular property calculations

5.3.1.1.1.a. Dipole moment

The values of *static* and *dynamic* dipole moment are given in **Table 5.1.** Since hyperpolarizability can be calculated as the second derivative of dipole moment, molecular design was concentrated on the molecules with higher dipole moment than the reactant molecule. As an established donor-π -acceptor system, PNA should possess a high dipole moment. From the CPHF-static calculations, the value obtained (7.9627D) is in good agreement with the experimentally determined value (7.2 D).[13] This also indicates the accuracy of CPHF calculation.

Table 5.1: Dipole moment of chromophores in units of debye

Chromophore	μ_x	μ_y	μ_z	μ_g *static*	μ_g *dynamic*
PNA	6.9218	0.0026	-3.9362	7.9627	43.6312
Tyr	1.9130	1.5148	2.0806	3.2068	20.5722
PNATY	2.1497	1.5269	4.7942	5.4715	34.9174
AZCl	1.3614	0.0012	0.0114	1.3615	10.6268
TYAZ	7.6858	3.2330	-0.1818	8.3400	87.0284
TYAZCl	10.1682	4.5984	-0.0456	11.1598	99.5583

L-tyrosine has been used as a chiral auxiliary. It does not possess a high value of dipole moment (3.2068 D). But the coupled product (PNATY) of L-tyrosine with PNA has shown dipole moment (5.4715 D) higher than L-tyrosine and the acylation product (TYAZ) has a dipole moment value (8.3400) higher than that of PNA itself. Chlorination of TYAZ was carried out for the ease of polycondensation with diol molecules. The chlorinated product TYAZCl has high dipole moment. Thus the calculated dipole moment values are in good agreement with the predicted route of design. The ZINDO-SOS *dynamic* calculation follows the same trend as that of the *static* calculation.

5.3.1.1.1.b. Polarizability (α)

The polarizability values are summarized in **Table 5.2.** It can be seen that the linear polarizability values increase with each forward step in the molecular design. The

coupled product (3.4544 esu) of PNA (1.3474 esu) and L-tyrosine (1.6613 esu) has higher alpha value than that of the reactants. The final acylated (9.6115 esu) and chlorinated (8.5721 esu) products are also showing good alpha values compared with the reactant molecules. This indicates that the designed route is exactly following the goal of designing highly active chromophores for NLO applications.

Table 5.2: Polarizability α of chromophore

Chromophore	α_{xx}	α_{yy}	α_{zz}	α *(au)*	α_{tot} $x10^{-23}$ *Static**	α_{tot} * $x10^{-23}$ *Dynamic**
PNA	121.6103	48.72226	102.4463	90.9263	1.3474	411.0
Tyr	132.5928	81.87931	121.8485	112.1067	1.6613	294.0
PNATY	221.9997	122.9558	354.3746	233.1100	3.4544	866.0
AZCl	202.9226	102.1023	389.5218	231.5155	3.4307	927.0
TYAZ	545.6926	587.1834	812.9603	648.6121	9.6115	1350.0
TYAZCl	505.0923	528.5364	701.7857	578.4714	8.5721	1430.0

**α (esu) = 0.148185x10^{-24} α (au)*

5.3.1.1.1.c. Hyperpolarizability (β)

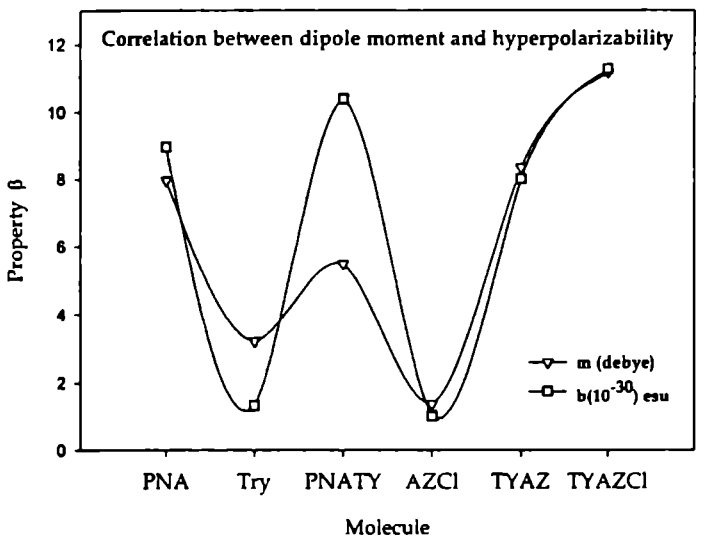

Figure 5.2. Correlation between dipole moment and hyperpolarizability

The *static* β values of chromophores are summarized in **Table. 5.3** *Static* CPHF calculation of hyperpolarizability values has followed the designed route (based on the dipole moment). (**Figure 5.2.**). Combination of PNA and Tyr produces a very good chromophore

PNATY with a good value of beta (10.374*10-30 esu). The *static* β value of TYAZ is not high as expected. The β value decreases after the acylation. This can be an inadequacy of *static* method due to the lack of including frequency in the calculation.

Table 5.3: HOMO-LUMO Gap (ΔE) in eV, Ground-State Dipole Moment (μ_g) in debye, Linear Polarizability (α) in units of 10^{-23} esu, and First Hyperpolarizability β, in units of 10^{-30} esu for the chromophores (ab initio CPHF static property calculations)

Chromophore	ΔE	μ_g	α	β
PNA	0.3507	7.9627	1.3474	8.9445
Tyr	0.3461	3.2068	1.6613	1.3165
PNATY	0.3248	5.4715	3.4544	10.374
AZCl	0.3309	1.3615	3.4307	1.0072
TYAZ	0.3264	8.3400	9.6115	8.0164
TYAZCl	0.3320	11.1598	8.5721	11.2620

Table 5.4: Oscillator strength f, Optical Gap (δE) in eV, Ground-State Dipole Moment (μ_g) in debye, Difference in dipole moments between ground state and excited state ($\Delta\mu$), Linear Polarizability (α) in units of 10^{-23} esu, and First Hyperpolarizability, in units of 10^{-30} esu for the chromophores (ZINDO SOS dynamic property calculations)

Chromophore	f	δE	$\Delta\mu$	μ_g	α	β_{vec}
PNA	1.0285	7.4823	14.1337	43.6312	411.0	220.3553
Tyr	1.2761	7.6630	6.6922	20.5722	294.0	51.1458
PNATY	0.9677	4.0466	28.1308	34.9174	866.0	226.5886
AZCl	1.3355	4.1932	3.3658	10.6268	927.0	106.8586
TYAZ	2.6372	4.4560	19.9043	87.0284	135.0	655.9493
TYAZCl	1.7055	4.4863	43.3013	99.5583	143.0	740.2353

In the *dynamic* ZINDO calculation the values are in good agreement with the proposed route. The acylated product, TYAZ and its chlorinated compound TYAZCl have shown the β values almost 3 times greater than PNATY. The results of dynamic ZINDO calculations are shown in **Table 5.4**. Even though the oscillator strength, f, of PNATY is small compared to all other molecules, the difference in dipole moment $\Delta\mu$ is

very large in this molecule. On the other hand, in TYAZ $\Delta\mu$ is smaller than PNATY, while the oscillator strength is the highest for this molecule. Thus, even by considering the ground state dipole moments can do prediction of the properties of the chromophore. But the exact picture of accurate and experimentally comparable results will be obtained from the *static* and *dynamic* calculations.

5.3.1.1.1. d. Chiral component

Table 5.5: *First hyperpolarizabilities of chromophores β (Static) in units of au*

β Tensors	*PNA*	*Tyrosine*	*PNATyr*	*AZCl*	*TYAZ*	*TYAZCl*
β_{xxx}	-713.4750	119.0279	72.9380	35.5150	-139.2570	-315.5060
β_{xxy}	0.0115	-8.1672	-10.9721	0.0007	463.1576	572.7625
β_{xyy}	38.5631	-10.7579	-15.0280	20.2807	-357.8430	-390.9130
β_{yyy}	0.1010	-27.8040	-20.0548	0.0498	-575.2070	-816.2450
β_{xxz}	620.9343	102.4751	281.3565	-1.9033	-368.2410	-515.5590
β_{xyz}	0.0481	21.6840	20.3777	-0.0641	402.8543	476.3268
β_{yyz}	-21.9295	-13.2235	46.7160	-0.0040	350.8687	497.3552
β_{xzz}	-225.082	26.5210	-1.5624	60.3724	-395.2590	-513.6710
β_{yzz}	0.0690	3.5213	-30.5448	0.1063	-126.9660	-210.4860
β_{zzz}	-87.2027	-26.0064	-1525.99	-7.9310	104.5484	86.4357
β_X	-899.9940	134.7910	56.3476	116.168	-892.3590	-1220.09
β_Y	0.1816	-32.4499	-61.5717	0.1568	-239.0150	-453.9680
β_Z	511.8021	63.2451	-1197.92	-9.8383	87.1761	68.2322
β_{vec}(au)*	1035.3410	152.3862	1200.826	116.584	927.9181	1303.596
β_{vec}(esu)*	8.9400	1.3200	10.4000	1.0100	8.0200	11.3000
% chirality	0.0046	14.4496	1.6969	0.0549	43.4148	36.5394

β (10^{-32} esu) = 0.863916β (au)

As explained in chapter 4, chiral component β_{xyz} plays an important role in the total macroscopic second harmonic generation efficiency χ_{XYZ}. Since present chapter is mainly on the design of efficient chiral chromophores for the synthesis of polymers so as

to obtain highly efficient chiral polymeric material, it is necessary, to get a good idea about the chiral component β_{xyz}. Values of all the β tensor components of the molecules are summarized in **Table 5.5.** It can be seen that, the chiral tensor β_{xyz} component of chiral molecules are very large compared to that of the achiral molecules. The β_{xyz} of PNA and AZCl is almost zero while that of TYAZCl is very large (percentage chirality is 43.41%). Thus, from the *static* and *dynamic* calculations, it can be concluded that the molecule TYAZCl, designed based on L-tyrosine framework will give polymers with very high macroscopic NLO response by contributing a major amount from the chiral nature

5.3.1.2 Diol molecules

Chiral diols

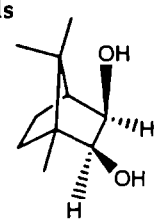

(1R, 2*S*, 3*R*, 4*S*)-Camphanediol

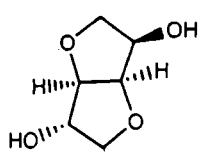

Isosorbide

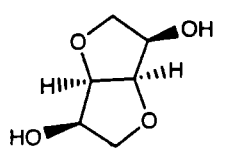

Isomanide

Achiral diols

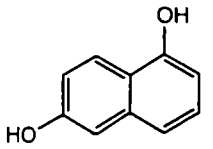

1,6-dihydroxy naphthalene (DN)

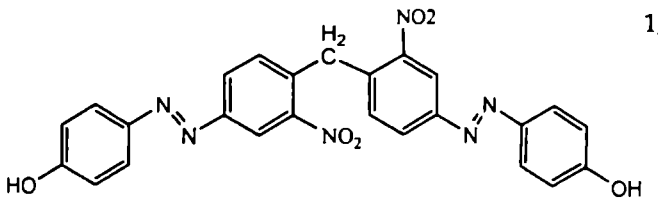

BHDM

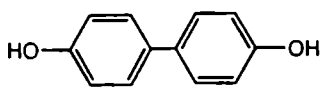

4,4'-dihydroxy biphenyl (DB)

Figure 5.3. Diol molecules

The diol molecules have been designed for the purpose of designing of polymer by easy polycondensation with the previously designed L-tyrosine based chromophore. The effect of chiral and achiral diol incorporation into a chiral medium has also been

studied. Keeping both these aspects, six diol molecules have been selected. Three chiral diols such as (1R, 2S, 3R, 4S) camphanediol (exo-exo-camphanediol), isosorbide and isomanide and three achiral diols such as bis(4-hydroxyphenylazo) 2,2'-dinitrodiphenylmethane (BHDM), 4,4'-dihydroxy biphenyl and 1,6-dihydroxy naphthalene. The structures of the diol molecules are given in **Figure 5.3**.

5.3.1.2.1. Static and Dynamic molecular property calculations

5.3.1.2.1.a. Dipole moment

The dipole moment values of diol molecules are summarized in **Table 5.6.** In *static* calculation, the chiral diol molecules have almost the same range of dipole moment values (≈3.5D). The achiral diols have dipole moments ranging from 1D to 4D. Thus diol molecules with dipole moments ranging from 1D to 4D were selected for designing polymers. Since CPHF *ab initio* calculation is the one which gives the accurate and more precise results, designing was always done based on the CPHF values, while dynamic ZINDO-SOS will give the experimental trend. From the table, it is clear that even though dipole moment values are very different in both calculations (*static* and *dynamic*) the trend is same in both cases. In the diastereomers, isosorbide and isomanide, isosorbide has more dipole moment than isomanide.

Table 5.6: Dipole moment of diols in units of debye

Diols	μ_x	μ_y	μ_z	μ_g *static*	μ_g *dynamic*
Camphanediol	-2.5764	1.3194	1.4803	3.2512	18.8980
Isosorbide	1.9131	-1.9957	1.8971	3.6529	20.8563
Isomanide	1.2125	-3.3750	0.3430	3.3025	20.4036
BHDM	-3.4635	-0.2513	-3.1963	4.7197	40.7927
DB	2.4287	-1.0047	0.0164	2.6284	15.7150
DB	1.0882	-0.0012	-1.4253	1.7933	8.8863

5.3.1.2.1.b. Polarizability

In *static* calculation, linear polarizability of diol molecule follows almost the same trend as that of dipole moment. In chiral diol molecules, camphanediol has shown maximum alpha values. (Comparable with the B3LYP/6-31+G (d,p) *static* and *dynamic* calculation in chapter 4) In *dynamic* calculation, α of 4, 4'-dihydroxy biphenyl is greater than 1,6-dihydroxy naphthalene. The α values of achiral diols are large compare to the chiral ones. The polarizability values are tabulated in **Table 5.7.**

Table 5.7: Polarizability α of diols

Diol	α_{xx}	α_{yy}	α_{zz}	*α (au)*	α_{tot} *x10*$^{-23}$ *Static**	α_{tot} * *x10*$^{-23}$ *Dynamic**
Camphanediol	107.9886	111.1823	104.4454	107.8721	1.5985	37.00
Isosorbide	78.7438	69.8929	68.9770	72.5379	1.0749	30.30
Isomanide	78.5334	69.5514	68.4718	72.1855	1.0697	31.10
BHDM	277.3586	565.2625	327.4995	390.0402	5.7798	80.00
DB	123.6634	92.0073	201.3266	138.9990	2.0598	82.00
DN	129.3573	63.4897	157.5047	116.7839	1.7306	96.00

5.3.1.2.1.c. Hyperpolarizability

The hyperpolarizability(β) values obtained by *static* calculation of chiral and achiral diols are given in **Table. 5.8**. In the case of diol molecules, the β values are not in line with the dipole moment values as in the case of chromophore design. The β value of BHDM is very low from the expected value on the basis of dipole moment, where as 1,6-dihydroxy naphthalene has shown maximum value of β irrespective of its low dipole moment. It can be seen from the **Table 5.8** that the HOMO-LUMO gap is the smallest in 1,6-dihydroxy naphthalene. Hence, charge transfer is easier in this molecule than any other diol and gives highest β value compared to all other diols concerned. The stereochemical effect explained in chapter 4 is prominent here also. The isomanide molecule is giving β value higher than its diastereomer, isosorbide. There is not much difference in β values with respect to chirality of the diols.

In *dynamic* calculation (**Table 5.9**) 1,6-dihydroxy naphthalene has shown a large β value compared to all other diols. It is surprising that in spite of a small difference in dipole moment $\Delta\mu$ (0.0011D), its β value is considerably large (115.4206*10 $^{-30}$ esu). While observing all other determining two-level parameters of β, it is clear that oscillator strength, which determines the transition probability, is comparatively high (6.6727eV) for this molecule.

Table 5.8: HOMO-LUMO Gap (ΔE) in eV, Ground-State Dipole Moment (μ_g) in debye, Linear Polarizability (α) in Units of 10^{-23} esu, and First Hyperpolarizability β, in Units of 10^{-30} esu for the diols (ab initio CPHF static property calculations)

Diol	ΔE	μ_g	α	β
Camphanediol	0.4316	3.2512	1.5985	1.4982
Isosorbide	0.4463	3.3529	1.0749	0.9714
Isomanide	0.4639	3.6025	1.0697	1.3064
BHDM	0.3350	4.7197	5.7798	1.4805
DB	0.3235	2.6283	2.0598	0.3914
DN	0.3195	1.7933	1.7306	2.3376

Table 5.9: Oscillator strength f, Optical Gap (δE) in eV, Ground-State Dipole Moment (μ_g) in debye, Difference in dipole moment between ground state and excited state ($\Delta\mu$), Linear Polarizability (α) in units of 10^{-23} esu, and First Hyperpolarizability, in units of 10^{-30} esu for the diols (ZINDO-SOS dynamic property calculations

Diol	f	δE	$\Delta\mu$	μ_g	α	β_{vec}
Camphanediol	0.0421	13.1441	-5.8724	18.8980	37.00	2.1819
Isosorbide	0.0359	11.3503	-0.3471	20.4563	30.30	3.2231
Isomanide	0.0710	11.0648	29.9015	20.8036	31.10	4.7217
BHDM	1.3825	4.6927	19.6174	40.7927	400.0	188.9864
DB	1.4738	7.2836	-0.0003	15.7149	482.0	2.5727
DN	6.6727	1.6507	0.0011	8.8863	496.0	115.4206

Also, the optical gap, δE, which determines the energy gap between the ground state and the lowest dipole allowed excited state, is very small. Thus charge transfer is easier in

this diol and gives rise to high second order response. Here also, the effect of stereochemistry of the molecule on the value of β is observed with the diastereomers, isosorbide and isomanide.

5.3.1.2.1.d. Chiral component

The chiral tensor components β_{xyz} are given in **Table 5.10**. The β_{xyz} values of the chiral diols are considerably large (3.5 -5 %) compared to achiral diols. In dihydroxy naphthalene it is negligible (0.0071%), while in biphenyl, it is almost comparable with the chiral diols (2.7909 %). This may be ascribed to the prochiral nature of biphenyl ring due to atropisomerism.[14]

Table 5.10: *First hyperpolarizability of chromophores β (Static) in units of au*

β Tensors	Camphanediol	Isosorbide	Isomanide	BHDM	DB	DN
β_{xxx}	-10.6371	73.9567	43.0462	216.3546	18.7792	20.9918
β_{xxy}	43.8721	-9.3928	-37.2348	102.2397	-2.1011	-0.0338
β_{xyy}	1.8530	6.3835	3.9828	835.5654	6.1059	-42.8274
β_{yyy}	94.7726	-56.6015	-96.6737	319.2446	-7.8695	-0.0172
β_{xxz}	22.7889	23.1046	7.8848	60.2572	-19.4143	141.7935
β_{xyz}	-6.9460	5.9513	-5.1115	-10.5550	-1.2643	-0.0194
β_{yyz}	3.8116	5.4817	4.1440	874.8085	19.3518	-30.3861
β_{xzz}	2.8651	1.3445	3.8377	135.5568	16.9497	-77.9663
β_{yzz}	24.1143	4.0012	-7.7733	-174.7390	-7.4174	-0.0252
β_{zzz}	32.9739	17.5415	2.3473	275.6137	0.3694	-362.9200
β_X	-5.9190	81.6848	50.8667	1187.4768	41.8349	-99.8018
β_Y	162.7591	-61.9931	-141.6820	246.7453	-17.3880	-0.0761
β_Z	59.5744	46.1280	14.3761	1210.6794	0.3069	-251.5130
β_{vec}(au)*	173.4205	112.4426	151.2212	1713.6887	45.3056	270.5901
β_{vec}(esu)*	1.5000	0.9714	1.3100	1.4805	0.3910	2.3400
%chirality	4.0052	5.2927	3.8014	0.6159	2.7909	0.0071

β (10^{-32} esu) = 0.863916β (au)

5.3.2 Polymer design

Design of polymers was based on the polycondensation of TYAZCl with the previously designed chiral and achiral diols. The repeating unit contains one TYAZCl molecule and one diol molecule. All calculations have been performed for three repeating units. The polymers are shown in **Figure 5.4** and **Figure 5.5**. SHG property has been compared with respect to 2-Methyl, 4-nitroaniline (MNA) as the reference material. MNA and polymers were optimized and properties were calculated using common level theory so as to avoid geometry effects in predictions.

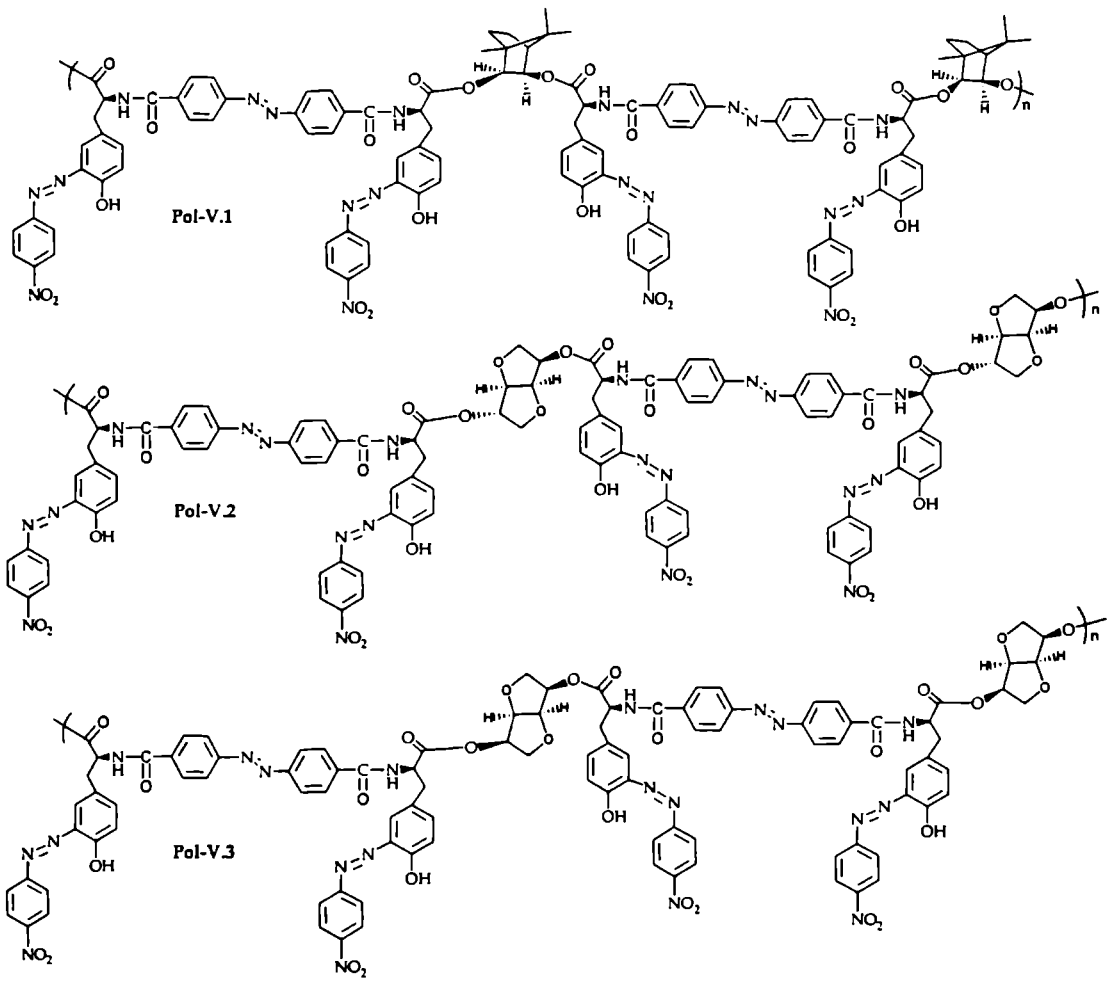

Figure 5.4. Structure of Chiral diol (2 repeating units) incorporated polymers (**Pol-V.1, Pol-V.2, Pol-V.3**)

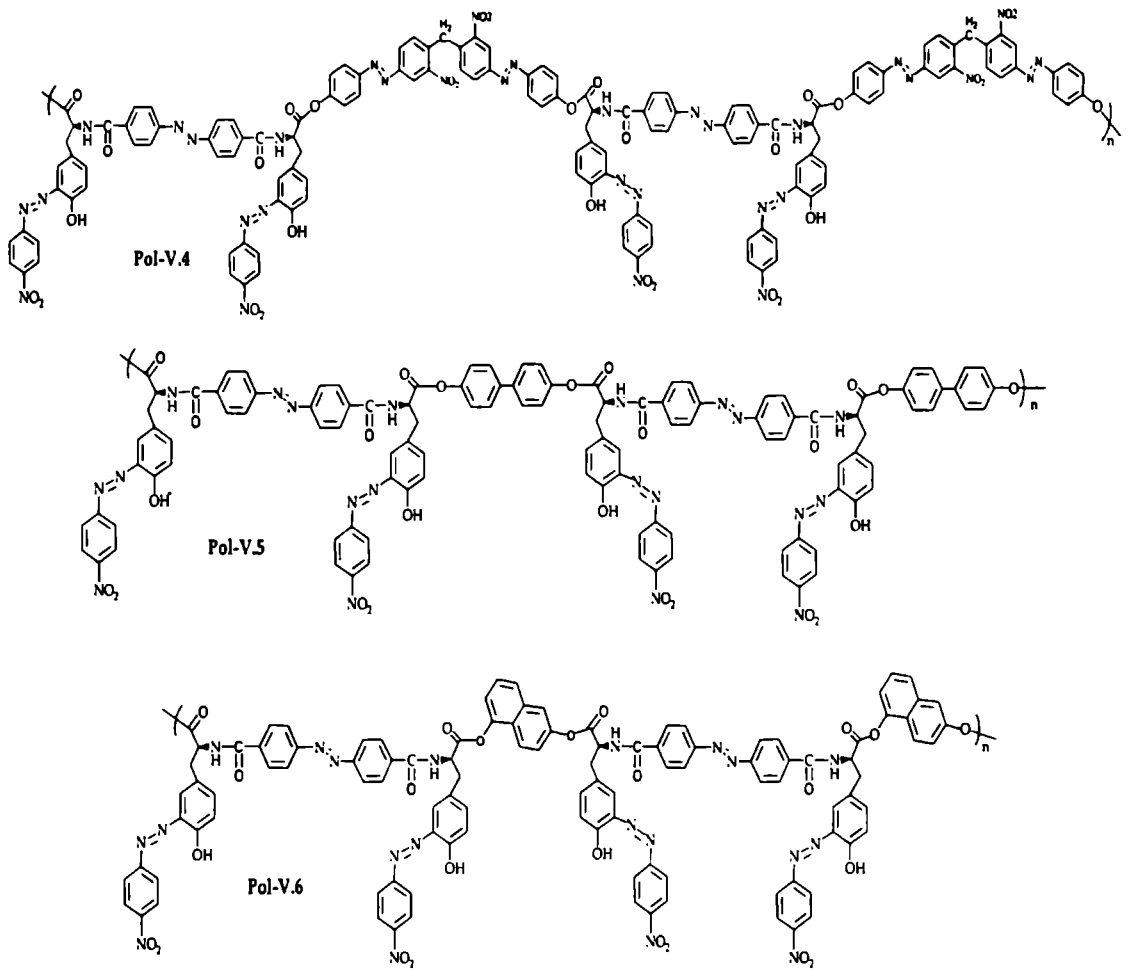

Figure 5.5. Structure of achiral diol (2 repeating units) incorporated polymers (**Pol-V.4, Pol-V.5, Pol-V.6**)

5.3.2.1 Static and dynamic molecular property calculations

5.3.2.1.a Dipole moment

All the polymers have shown large dipole moments compared to MNA (≈ 5 times). Chirality of chiral diol hasn't affected the dipole moment. Both types of polymers, the one designed from chiral diol and those designed from achiral diol have shown similar values of dipole moment. The dipole moment values of polymers are presented in **Table 5.11**.

Table 5.11: Dipole moment values of polymers in units of debye

Polymers	μ_x	μ_Y	μ_Z	μ_g *Static*	μ_g *Dynamic*
Pol-V.1	19.7620	8.7396	-0.8627	21.6255	242.1503
Pol-V.2	38.5563	6.7376	0.4145	39.1428	572.2634
Pol-V.3	26.9111	6.0175	-1.2337	27.6033	286.6680
Pol-V.4	8.5608	25.3201	-15.6744	30.9859	423.9742
Pol-V.5	34.1279	15.2220	-0.0963	37.3689	355.5187
Pol-V.6	29.3493	13.4670	-0.2270	32.2923	332.3781
MNA	0.1357	1.3755	-6.8645	7.0023	40.0614

5.3.2.1.b Polarizability (α)

Linear polarizability values are shown in **Table 5.12**. The chirality of the constituent diols has not affected the polarizability values. The structure of the polymers showed increased polar order by virtue of having greater contribution from the dipolar chromophoric groups (both azo group and amino-nitro group). All the polymers incorporated with chiral or achiral diols have shown the polarizablity values in the same range (~$35x10^{-23}$ esu in *static* calculation). Both the calculations have shown that the present series of polymers have very high α values with respect to MNA. These indicate that these polymers can be used for optical devices.

Table 5.12: Polarizability (α) of polymers

Polymers	α_{xx}	α_{yy}	α_{zz}	α *(au)*	α_{tot} $x10^{-23}$ *Static**	α_{tot} * $x10^{-23}$ *Dynamic**
Pol-V.1	2022.926	2224.921	2758.197	2335.348	34.606	4056.48
Pol-V.2	1752.230	2303.824	2468.601	2174.885	32.229	152.928
Pol-V.3	1759.414	2276.693	2437.519	2157.875	31.977	3340.80
Pol-V.4	2637.1810	2438.77	2499.221	2525.057	37.410	3250.46
Pol-V.5	1952.120	2572.932	3032.917	2519.323	37.333	3421.44
Pol-V.6	1809.624	2338.003	2943.665	2363.764	35.028	3304.80
MNA	99.4808	38.78715	122.8410	87.036	1.290	400.0012

* α *(esu)* = $0.148185x10^{-24}$ α *(au)*

5.3.2.1.c Hyperpolarizability

Static (CPHF) hyperpolarizability values (**Table 5.13**) of polymers show a different trend compared to that of the dipole moment and polarizability trends. While dipole moment, μ_g and polarizability,α values are in a closer range for polymers the hyperpolarizability values varied from 14x 10^{-30} esu to 50x10^{-30} esu. The presence of chiral diols does not have any significant role in increasing the β value. Moreover, isosorbide (**Pol-V.2**) and isomanide (**Pol-V.3**) containing polymers have shown the lowest values of β. But in this case also, the stereochemical effect on β is prominent. Isomanide is giving higher β value than isosorbide as in all other cases. All the polymers have shown high value of β . Thus, it can be concluded that the L-tyrosine based chromophore is very efficient in designing good NLO active material with high SHG efficiency. Even though the variation of β can be related to the HOMO-LUMO gap and then to charge transfer, the change in β value is not directly proportional to the difference in energy gap.

Table 5.13: ***HOMO-LUMO Gap(ΔE) in eV, Ground-State Dipole Moment (μ_g) in debye, Linear Polarizability (α) in units of 10^{-23} esu, and First Hyperpolarizability β, in units of 10^{-30} esu for the polymers (ab-initio CPHF static property calculations)***

Polymers	ΔE	μ_g	α	β_{vec}
Pol-V.1	0.3134	21.6255	34.6060	35.9861
Pol-V.2	0.3343	39.1428	32.2290	14.4112
Pol-V.3	0.3374	27.6033	31.9770	18.8488
Pol-V.4	0.3243	30.9859	37.4100	26.9000
Pol-V.5	0.2925	37.3689	37.3330	33.6258
Pol-V.6	0.2836	32.2923	35.0280	34.7583
MNA	0.3970	7.0023	1.2898	5.2684

As described in previous chapters, based on two-level model, the trendsetters in the field of SHG are two-level parameters such as oscillator strength, *f*, optical gap, δE, and difference in dipole moment between ground state and excited state, $\Delta\mu$. Thus the

variation in β can be explained from the results obtained by *dynamic* ZINDO-SOS calculation.

Table 5.14: Oscillator strength (f), Optical Gap (δE) in eV, Ground-State Dipole Moment (μ_g) in debye, Difference in dipole moments between ground state and excited state ($\Delta\mu_g$), Linear Polarizability (α) in units of 10^{-23} esu, and First Hyperpolarizability, in units of 10^{-30} esu for the polymers (ZINDO-SOS dynamic property calculations)

Polymer	*f*	δE	$\Delta\mu$	μ_g	α	β_{vec}
Pol-V.1	5.3562	13.4529	133.6228	242.1503	405.648	2168.197
Pol-V.2	0.4684	17.7927	240.6799	572.2634	15.2928	762.805
Pol-V.3	5.0169	14.3649	142.4032	286.6680	334.080	1536.880
Pol-V.4	3.9045	15.0972	168.9320	423.9742	400.9702	1797.502
Pol-V.5	4.0649	13.8318	185.4564	355.5187	342.144	1966.639
Pol-V.6	4.1477	14.0781	126.1178	332.3781	330.480	1466.959
MNA	0.9502	8.2721	12.0416	39.5013	300.8571	182.464

From **Table 5.14,** it can be seen that all the polymers have shown high second order NLO response. **Pol-V.2** (isosorbide) has the lowest value of β and **Pol-V.1** (camphanediol) has the highest value ofβ. These results are also in agreement with the CPHF predictions. In **Pol-V.2** even though the difference in dipole moment $\Delta\mu$ is high, the oscillator strength is minimum compared to all other systems. Also, the optical gap,δE is the maximum in **Pol-V.2**. Since the charge transfer in molecules is determined by both these factors, low oscillator strength and high optical gap reduces the charge transfer considerably and hence the polymer **Pol-V.2** has the lowest SHG response. In **Pol-V.1**, which has the maximum value of β, the value of $\Delta\mu$ is less compared to **Pol-V.2**. But f is maximum and δE is the minimum for this polymer compared to all other polymers of this series. This facilitates easy charge transfer and hence high β value for this polymer. The β values of all other polymers are in accordance with the two-level parameters. The chiral diols does not have significant contribution to the trend for predicting the total β_{vec}. Since the medium is already chiral, by virtue of having the tyrosine unit, incorporation of an additional chiral unit does not play any important role in determining molecular second order response β_{vec}. But here also, the effect of

stereochemistry on β value is prominent and follows the same trend as described in chapter 4. The diastereomer, isomanide showed higher β value than its analogue isosorbide. This indicates that polar ordering is vital in any system whether it is chiral or not.

5.3.2.1.d Chiral component

Table 5.15: First hyperpolarizability (β) tensors (static) of Polymers in atomic units

β Tensors	Pol-V.1	Pol-V.2	Pol-V.3	Pol-V.4	Pol-V.5	Pol-V.6	MNA
β_{xxx}	-1048.33	500.3188	219.2635	503.6268	-997.694	-988.283	-24.4201
β_{xxy}	1677.457	921.6536	990.8157	274.3517	1827.039	1731.973	13.5831
β_{xyy}	-1200.67	-1551.85	-1841.85	129.2712	-1282.98	-1200.15	12.7643
β_{yyy}	-2466.73	-399.395	-920.593	239.5554	-2552.55	-2521.87	7.1032
β_{xxz}	-1509.88	-568.978	-611.594	2856.3440	-1525.00	-1474.58	-137.669
β_{xyz}	2389.433	1191.205	1234.665	983.1450	1406.965	1369.30	0.91896
β_{yyz}	1454.972	373.3215	613.6915	-973.1370	1440.737	1437.96	-26.7852
β_{xzz}	-1627.78	-561.931	-537.314	-329.5080	-1380.15	-1565.74	15.0009
β_{yzz}	-717.775	-109.928	-239.676	2485.3480	-577.409	-635.238	-20.2272
β_{zzz}	279.673	98.7310	255.3821	-1103.590	308.7788	286.566	774.273
β_X	-3876.78	-1613.46	-2159.9	303.3897	-3660.82	-3754.17	3.3450
β_Y	-1507.05	412.3308	-169.454	2999.2550	-1302.92	-1425.14	0.45917
β_Z	224.7625	-96.9257	257.4799	779.6211	224.5186	249.9474	609.819
β_{vec}(au)*	4165.467	1668.131	2181.788	3113.7410	3892.251	4023.337	609.8281
β_{vec}(esu)*	35.9861	14.4112	18.8488	26.9001	33.6258	34.7583	5.2684
%chirality	57.3629	71.4095	56.5895	31.2534	36.1478	34.0339	0.1506

** β_{vec} x 10^{-30}, β (10^{-32} esu) = 0.863916β (au)*

In all the polymers, the chiral tensor component β_{xyz} is much large. In **Pol-V.2** (Isosorbide) the percentage of chirality is more than 70%, while that of MNA is only 0.15%. This large increase in chiral component β_{xyz} is due to the basic L-tyrosine based framework of the polymers. This framework imparts chirality across the whole polymer

chain and increases the % chirality to a large extent. More over, the possible helical structure of the polymers contributes a considerable amount to the chirality (**Figure 5.18**). It is obvious that the % chirality and the value of β_{xyz} is more than 50% in polymers with chiral diols. For other diols it is only about 30%. Incorporation of chiral diol unit in to an already chiral medium increases the chiral tensor component. The large β_{xyz} component leads to large macroscopic chiral component χ_{xyz}, which is one of the major components of macroscopic hyperpolarizability. Thus, even though in the microscopic level total β_{vec} values, the contribution due to chiral diol incorporation in the chiral medium is negligible, the chiral incorporation will increase macroscopic second order susceptibility χ through large values of macroscopic chiral component χ_{xyz}.

5.4. Synthesis

A series of polymers based on L-tyrosine framework has been designed and the spectroscopic properties are calculated using *static* and d*ynamic* methods. Calculations reveal that all the polymers are good SHG active materials. So these polymeric structures were taken in to the laboratory for synthesis. Six polymers were synthesized having L-tyrosine framework and diols (chiral and achiral) by high temperature polycondensation method. The following section deals with the synthetic procedures.

5.4.1 Monomer synthesis

5.4.1.1 Synthesis and characterization of chiral chromophore

L-Tyrosine based chiral chromophore was synthesized by a two-step process. In the first stage L-tyrosine was coupled with *para* nitroaniline to get PNATY. In the second stage PNATY was acylated with 4'4' azobenzene dicarboxylic acid to get TYAZ. Chlorination of TYAZ yielded TYAZCl.

Synthesis of (S)-2-amino-3-(3-(4-nitrophenylazo), 4-hydroxyphenyl) propanoic acid (PNATY, 3) [15]

L-Tyrosine (Loba Chemie, 99% pure), *Para* nitroaniline (s. d. fine, 99% pure) Sodium nitrite (s. d. fine, 98% pure), Sodium acetate (s. d. fine 98% pure) were used for

IR(KBr pellet) cm^{-1} : 3076 (NH^+, NH st), 3115(-OH st), 2065 (distinct side band due to zwitter ion), 1719 (carbonyl), 1589 (COO^-), 1538 (NO_2 st as), 1510 (NH_3^+ δsy), 1429 (N=N- st), 1348 (-NO_2 st ay) 1275 (aromatic trans -N=N-)

^1H NMR (300 MHz DMSO-d_6) : δ 11.3 (carboxylic -OH), 9.1 (phenolic -OH), 8.5 (d, 2H, aromatic, near to NO_2, H1), 8.2 (d, 2H, aromatic, near to -N=N-, H2), 7.7 (d, NH_3^+), 7.4 (d, 1H, amino acid benzene ring near to -N=N-, H3), 7.1 (d, 1H, amino acid benzene ring near to -CH_2, H4) 6.7 (d, 1H, amino acid benzene ring near to -OH, H5), 4.1(t, I H, -CH), 3.1, 3.2 (d, 2H, -CH_2)

^{13}C NMR (75 MHz DMSO-d_6): δ 174.9 (-CO in $-COO^-$), 158.8 (aromatic C, -C-N=N-, C4), 150.6 (aromatic C, -C-NO_2, C1), 149.4 (C in amino acid phenyl, -C-OH,C7), 132.4 (C in amino acid phenyl, -C-CH_2, C10, 131.4 (C in amino acid phenyl near to CH_2,C9), 125.1 (C, in amino acid -C-N=N-, C6), 124. 7 (C in amino acid phenyl near to CH_2, C5), 123.9 (aromatic carbon near to -N=N-, C3), 121.4 (aromatic C near to -NO_2,C2), 116.1 (C in amino acid phenyl near to -OH, C8), 56.8 (C in -CH), 39.4 (C in -CH_2)

Mass (m/e): 330 (molecular ion), 301 (M-CHO), 285 (M-COOH), 150 (-N=N-$C_6H_5NO_2$), 122 (base peak, $C_6H_5NO_2$).

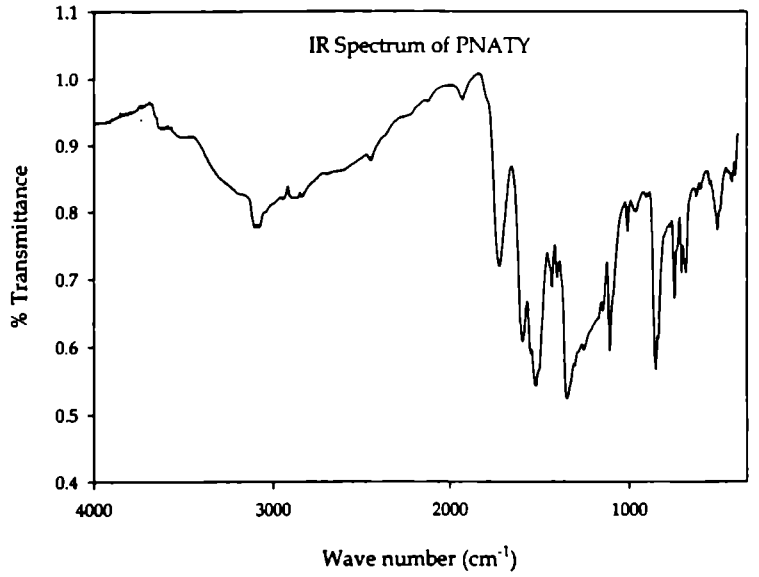

Figure 5.6. IR spectrum of PNATY

A peak between 370 and 379 nm in UV-VIs absorption spectrum is due to the azo group ($\pi \rightarrow \pi^*$) In IR spectrum (**Figure 5.6**) of PNATY, a distinct side band at 2065 cm^{-1} confirms the zwitter ion form of the amino acid moiety.[16] The NH stretching frequency at 3115 cm^{-1} instead of 3300-3500cm^{-1} indicates the

presence of NH_3^+ group.[17] The peak at 1719 cm^{-1} confirmed carbonyl absorption and peaks at 1538 and 1348 cm^{-1} confirmed-NO_2 group.

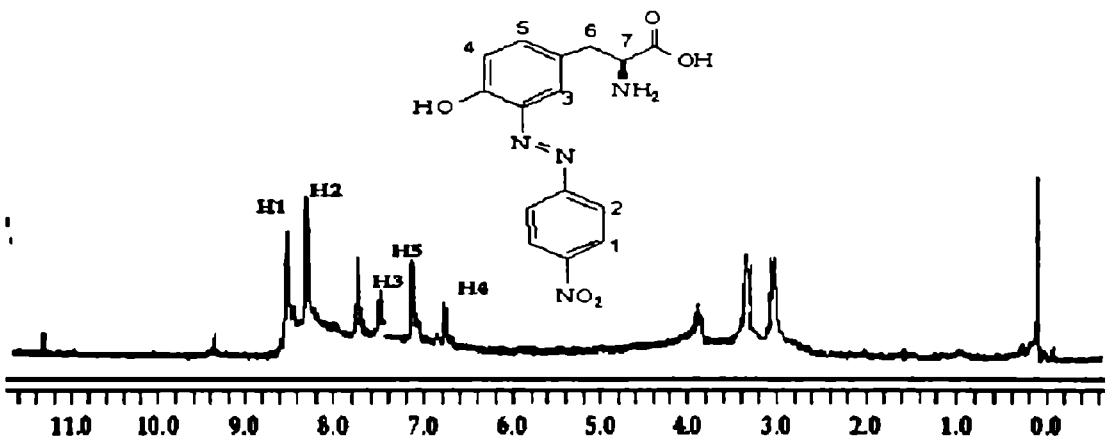

Figure 5.7. ^1H NMR spectrum of PNATY

In ^1H NMR spectrum (**Figure 5.7**) the doublet at 7.7 δ confirmed the presence of NH_3^+. Five doublets in the aromatic region confirm the presence of five different aromatic hydrogen. This confirms monosubstitution of PNA at tyrosine ring. If disubstitution had occurred (at C8 also), aromatic region would have shown only four aromatic peaks. The doublets at δ 3.1 and δ 3.2 confirms -CH_2 group and -CH proton triplet is seen at δ 4.1. Off scale peak at δ 11.3 indicates -COOH protons. -OH peak is seen at δ 9.1.

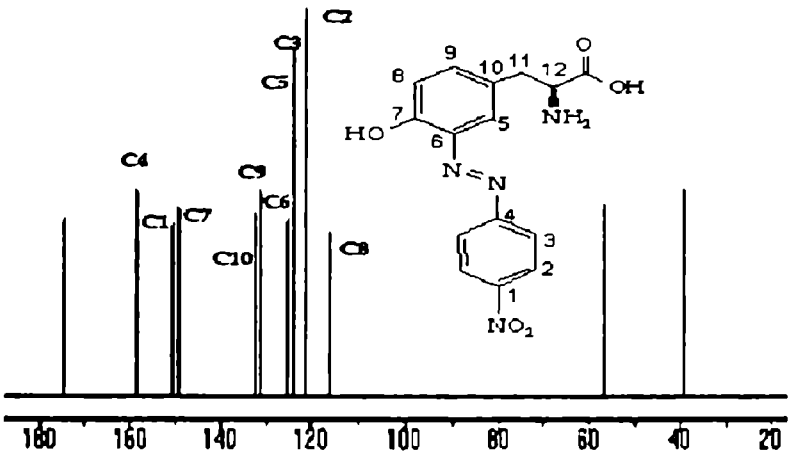

Figure 5.8. ^{13}C NMR of PNATY

Thirteen distinct carbons in ^{13}C NMR spectrum (**Figure 5.8**) confirm monosubstitution. If the substitution were at both the *meta* carbon of tyrosine ring, the ^{13}C NMR spectrum would have given only 12

distinct carbons.In the mass spectrum (**Figure 5.9**), molecular ion peak at m/e=330 once again confirms the monosubstitution. Peaks due to M - COOH at m/e 285, M-CHO at m/e 301 , $C_6H_5NO_2$ at m/e 122 and -N=N-$C_6H_5NO_2$ at 150 δ confirm the proposed structure for the compound.

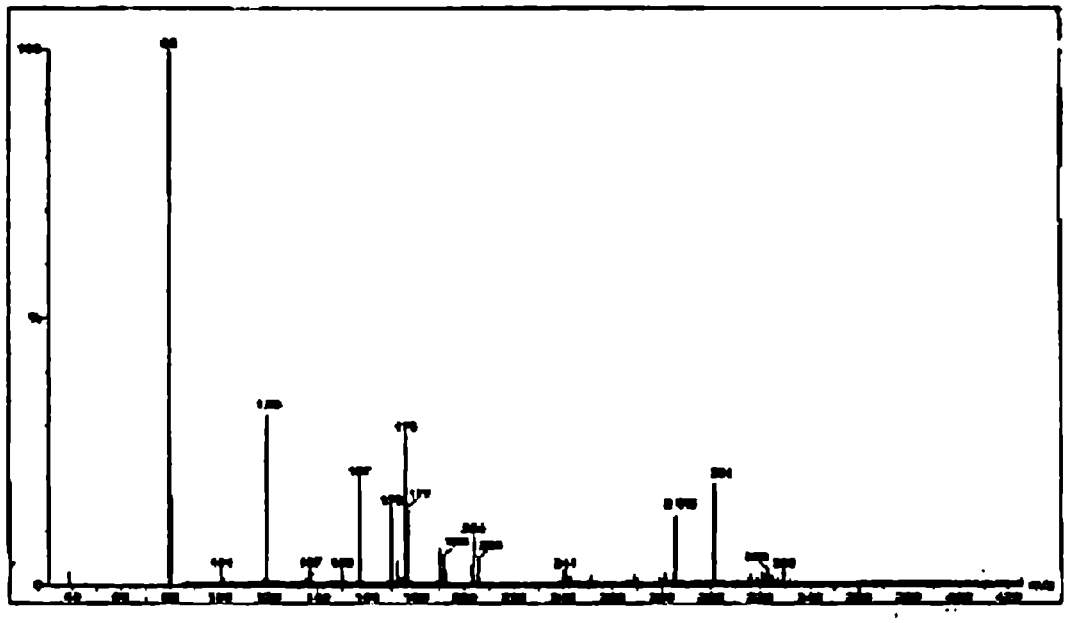

Figure 5.9 Mass spectrum of PNATY

Synthesis of bis[(S)-2-(4-azenyl benzamido)-3-(3-(4-nitrophenylazo), 4-hydroxyphenyl) propanoic acid chloride (TYAZCl, 6)

4,4' azobenzene dicarboxylic acid chloride (AZCl, **4**) and (S)-2-amino-3-(3-(4-nitrophenylazo)-4-hydroxyphenyl) propanoic acid (PNATY, **3**) were used for the synthesis of bis[(S)-2-(4-azenyl benzamido)-3-(3-(4-nitrophenylazo)-4-hydroxyphenyl) propanoic acid chloride (TYAZCl, **6**). Synthesis of acid chloride has been described in chapter 4

In to a 50 mL three necked round bottom flask equipped with mechanical stirring and heating, PNATY (1 g, .00316 mol) and 4,4'-azobenzene dicarboxylic acid chloride (AZCl, 0.484 g, 0.00158 mol) were added. THF (15 mL) was added as solvent. To this mixture few drops of pyridine were added. The reaction was carried out for 24h at

reflux temperature under nitrogen atmosphere. The reaction mixture was cooled and filtered. Dark brown solid of TYAZ was obtained. It was recrystalized from methanol. (M.P 144^0 C). The product TYAZ was refluxed with $SOCl_2$ for 24h under nitrogen atmosphere to obtain TYAZCl (**6**). The reaction mixture was cooled, filtered and recrystallized from acetone.

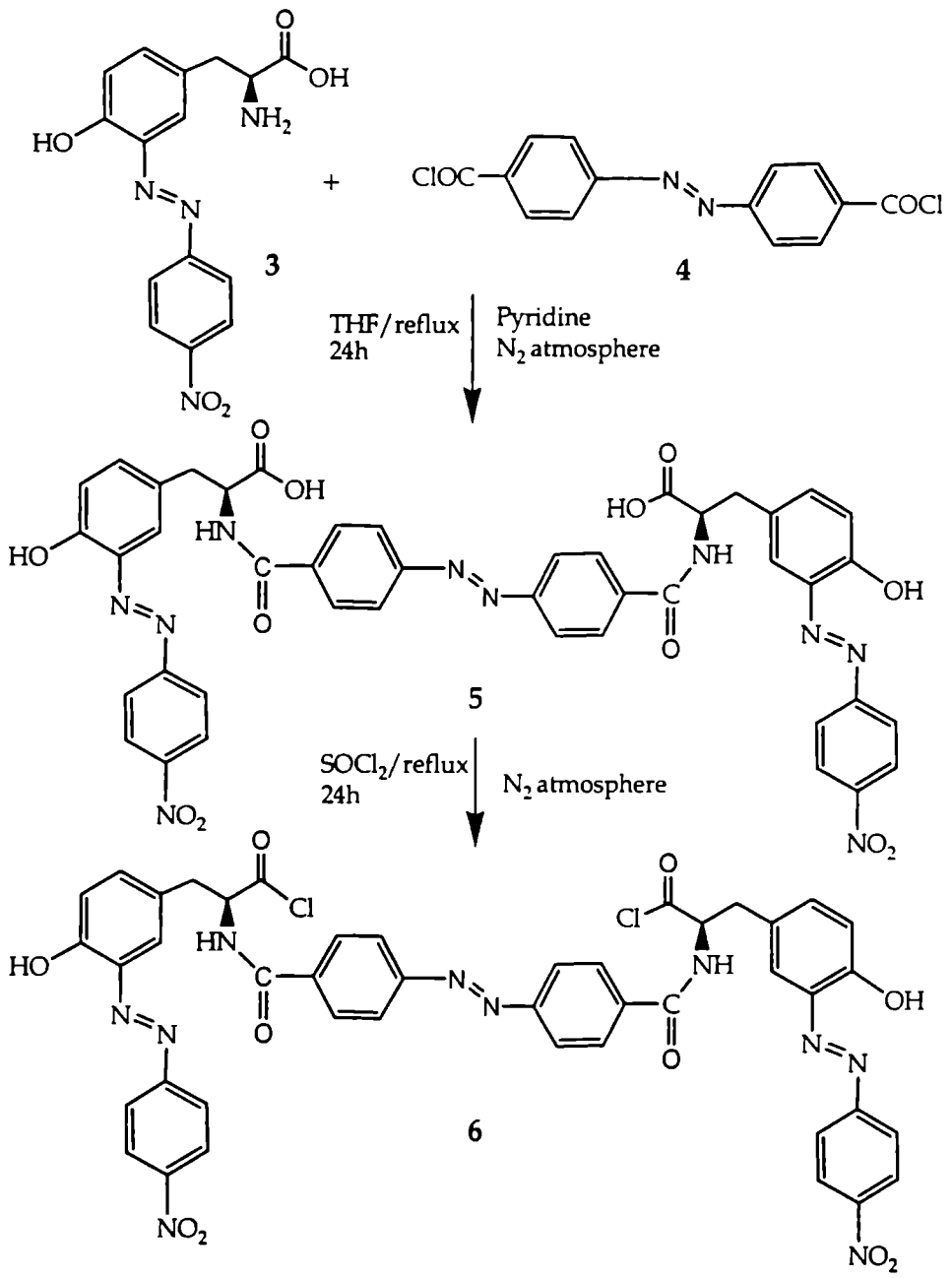

Scheme 5.2. Synthesis of TYAZCl

Characterization

Yield 86%, $[\alpha]_D$ -11.3^0 Decomposed at 231^0 C

Elemental analysis: Calculated for $C_{44}H_{32}Cl_2N_{10}O_{10}$ – C, 56.72; H, 3.46; N, 15.03. Found - C, 56.53; H, 3.45; N, 15.17

Spectral properties

UVλ_{max} (solid) nm: 300 (NO_2) 379 (-N=N-)

IR(KBr pellet) cm^{-1} : 3407 (O-Cl st), 3077(-OH st) 1740(carbonyl of acid chloride), 1689 (carbonyl of amide) 1530 (NO_2 st as), 1432 (-N=N- st) 1330(-NO_2 st ay) 1279 (aromayic trans -N=N-)

^{1}H NMR (300 MHz DMSO-d_6): δ 9.2 (2H, phenolic -OH), 8.39 (d, 4H aromatic, near to NO_2,H1), 8.3(4H aromatic, near to -N=N-,H2)8.17 (4H, aromatic hydrogen from acid chloride near to -CO,H8) 8.03 (4H, aromatic hydrogen from acid chloride near to -N=N, H9) 7.8 (d, 2H,amide hydrogen), 7.5 (d, 2H, amino acid phenyl ring near to -N=N-, H3), 7.0 (d, 2H, amino acid phenyl ring near to -CH_2, H5) 6.6 (d, 2H, amino acid benzene ring near to -OH), 4.3(m, 2H, -CH), 3.1, 3.2 (d, 4H, -CH_2)

^{13}C NMR (75 MHz DMSO-d_6): δ 173 (-CO, acid chloride), 167.6 (-CO, amide), 158.8, 156.1, 150.6, 149.4, 136.3, 132.4, 131.2, 127.8, 125.2, 124.7, 123.4, 121.5, 121.1, 116.1 (aromatic), 71.4 (-CH), 37 (-CH_2)

Mass: 930 (molecular ion), 360 (O_2N-Ph-N=N-Ph(OH)CH_2-CH(NH)Cl), 312 O_2N-Ph-N=N-Ph(OH)CH_2-CH(NH)), 236 (CO-Ph-N=N-Ph-CO)

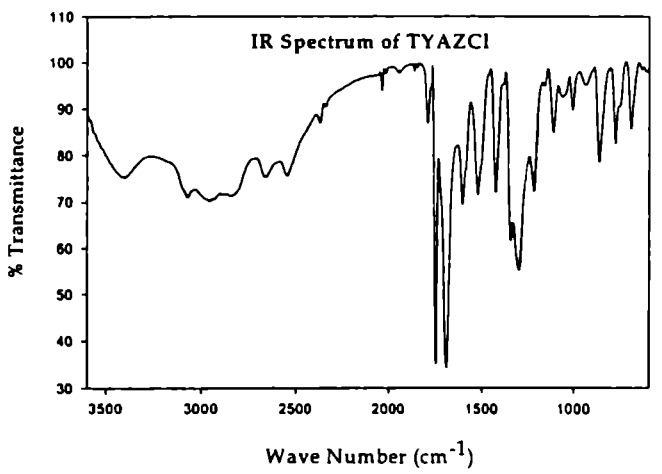

Figure 5.10. IR spectrum of TYAZCl

In the IR spectrum a structured band at 3407 cm^{-1} indicates the presence of O-Cl, hydrochloride of amino acids (confirmed chlorination of TYAZ). Two distinct bands at 1730 cm^{-1} and 1689 cm^{-1} indicate two type of

carbonyl functionality. The band at 1730 cm^{-1} is due to the carbonyl of acid chloride and the later at 1689 cm^{-1} is due to the amide carbonyl. This has confirmed the amide formation.

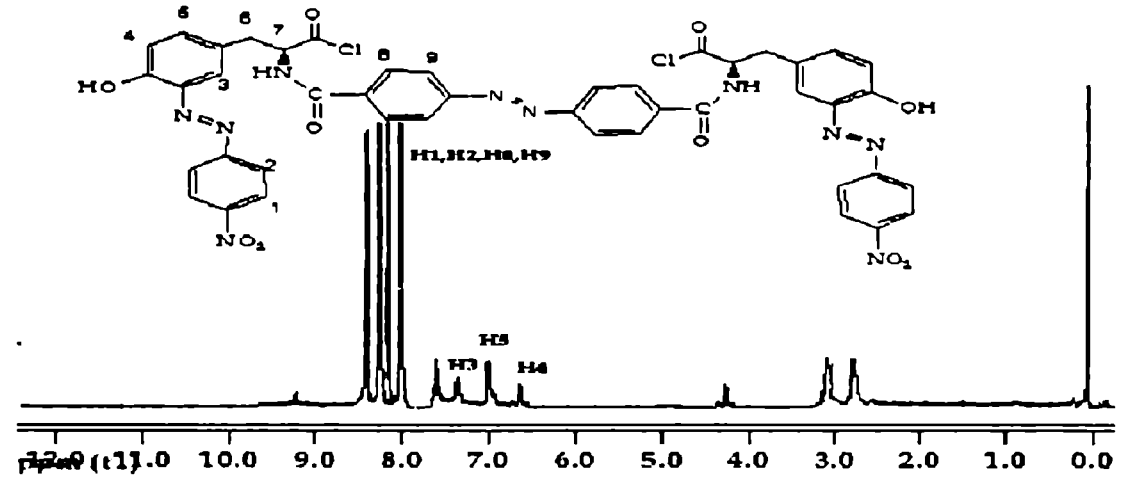

Figure 5.11. ^{1}HNMR spectrum of TYAZCl

Seven different types of hydrogens confirmed the disubstitution at azo acid chloride. Monosubstitution would have given nine different hydrogens. Absence of off field peak has confirmed the absence of carboxylic -OH hydrogen and has thus confirmed chlorination. The peak due to -CH hydrogen was shifted to δ 4.8 which is due to the presence of -COCl near to -CH.

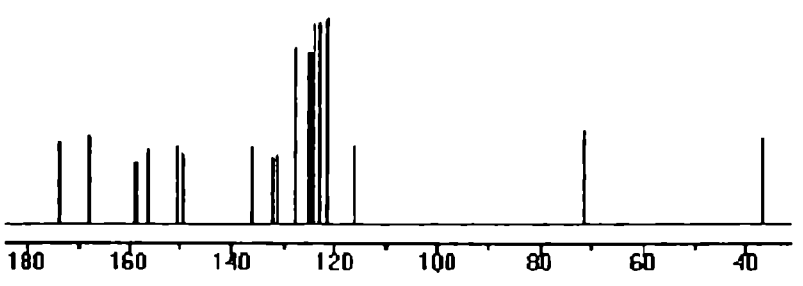

Figure 5.12. ^{13}C NMR spectrumof TYAZCl

Fourteen carbons in the aromatic region could confirm disusbstitution at the acid chloride part. The peaks at δ 167.6 (due to amide group) and peak at δ 173.6 (due to carboxylic -CO) also could confirmed two different carbonyl groups and have confirmed the proposed structure.

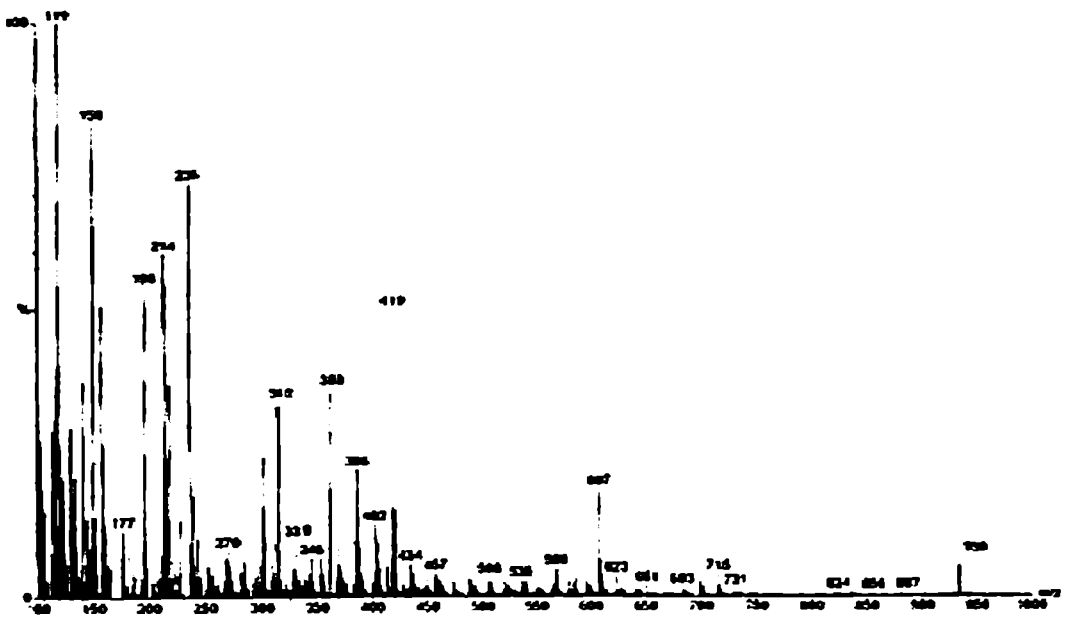

Figure 5.13 Mass spectrum of TYAZCl

5.4.2 Polymer Synthesis

Previously designed polymer structures were synthesized by the polycondensation of L-tyrosine based chromophore with the diols. All polymer syntheses were done by solution method at high temperatures. Appropriate diol molecule was dissolved in extremely dry dimethyl actamide (HPLC grade, s. d. fine). To this solution, bis{(S)-2-(4-azenyl benzamido)-3-(3-(4-nitrophenylazo), 4-hydroxyphenyl) propanoic acid chloride (TYAZCl, 6) dissolved in DMAc was added. Few drops of extremely dry pyridine (99.99% dry pyridine, s. d. fine) were added as acid acceptor. The mixture was refluxed under stirring for 25h. The product was precipitated from cold methanol and washed continuously with hot water, methanol and acetone. After filtration and drying a brown solid was obtained. **Scheme 5.3** gives the synthetic route of polymers.

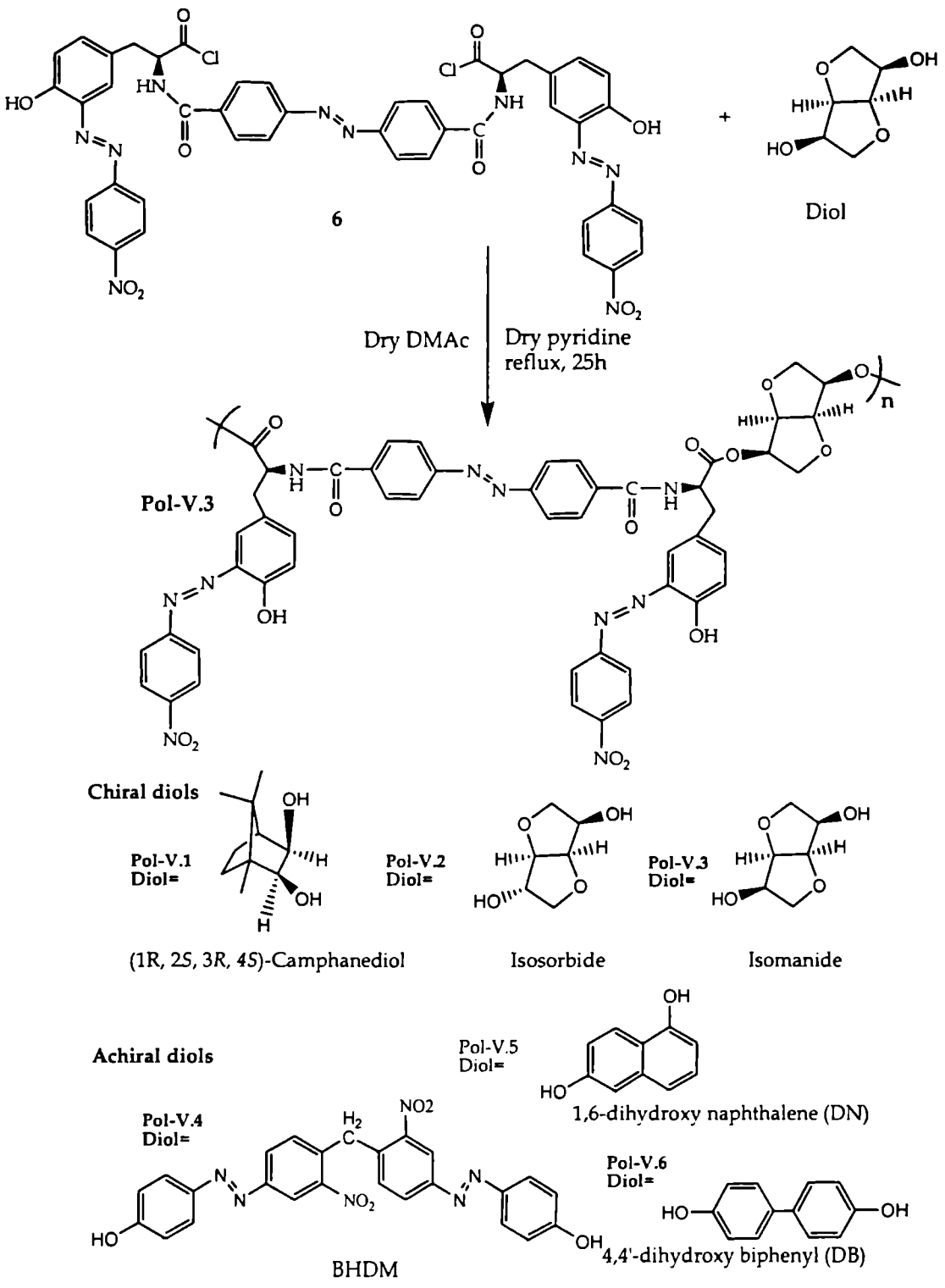

Scheme 5.3 Synthesis of poly (ester-amide) s

5.4.2.1. Characterization of polymers

Pol-V.1

Yield: 71%

Spectral properties

UVλ_{max} (solid): 362 ($\pi \rightarrow \pi^*$, N=N) 323 ($n \rightarrow \pi^*$, NO_2)

IR(KBr pellet) cm^{-1} : 3393 (NH st, OH st), 2921 (-CH stretch in camphanediol), 1730 (aromatic ester carbonyl), 1685 (amide I carbonyl stretch), 1530 (NO_2 st as, amide II st sy), 1423 (-N=N- st), 1349 (NO_2 st sy)

^{1}H NMR (300 MHz DMSO-d_6): δ 9.2 (phenolic -OH), 8.4 (aromatic, near to NO_2), 8.1(4H aromatic, near to -N=N-), 7.8 (aromatic hydrogen from ester amide near to -CO), 7.5 (aromatic hydrogen from ester amide near to -N=N-), 7.3 (amino acid phenyl ring near to -N=N-), 7.1 (amino acid phenyl ring near to $-CH_2$), 6.7 (amino acid phenyl ring near to -OH), 4.8(m, -CH), 4.2, 4.3 (d, $-CH_2$), 3.1 (m, $-CH_2$ cyclopentane ring of camphanediol), 2.4 (m, -CH, cyclopentane ring of camphanediol), 2.1 (s, $-CH_3$ of camphanediol), 1.24 (s, bridged $-C(CH_3)_2$ of camphanediol).

Pol-V.2 and Pol-V-3

Pol-V.2 (Yield 78%) and **Pol-V.3** (yield 75%) are different only in the stereochemistry of the chiral building units. So their spectral patterns are similar except in ^{1}HNMR. But in ^{1}H NMR the -CH protons which have the different stereochemistry in isosorbide and isomanide appeared as multiplet. So a distinction between them is difficult.

Spectral properties

UVλ_{max} (solid): 362 ($\pi \rightarrow \pi^*$, N=N), 323 ($n \rightarrow \pi^*$, NO_2)

IR (KBr pellet) cm^{-1} : 3393 (NH st, OH st), 2921 (sp^3 -C-H stretch in isosorbide or isomanide unit), 1730 (aromatic ester carbonyl), 1685 (amide I carbonyl stretch), 1530 (NO_2 st as, amide II st sy), 1423 (-N=N- st), 1349 (NO_2 st sy), 1235-1240 (C-O st in isosorbide or isomanide unit)

^{1}H NMR (300 MHz DMSO-d_6): δ 9.2 (phenolic -OH), 8.4 (aromatic, near to NO_2), 8.1(4H aromatic, near to -N=N-), 7.8 (aromatic hydrogen from ester amide near to -CO), 7.5

(aromatic hydrogen from ester amide near to -N=N-), 7.3 (amino acid phenyl ring near to -N=N-), 7.1 (amino acid phenyl ring near to $-CH_2$) 6.7 (amino acid phenyl ring near to -OH), 4.8(-CH), 4.2, 4.3 ($-CH_2$), 4.0 (-CH isosorbide or isomanide unit), 3.5 ($-CH_2$ in isosorbide or isomanide unit), 3.3 (bridge CH in isosorbide or isomanide unit)

Pol-V-4

Yield: 74%

Spectral properties

UVλ_{max} (solid): 274 (-Ph-CH_2-Ph-), 362 ($\pi \rightarrow \pi^*$, N=N), 323 ($n \rightarrow \pi^*$, NO_2)

IR(KBr pellet) cm^{-1} : 3393 (NH st, OH st), 947 (CH_2 in Ph-CH_2-Ph), 1730 (aromatic ester carbonyl), 1685 (amide I carbonyl stretch), 1530 (NO_2 st as, amide II st sy), 1423 (-N=N- st), 1349 (NO_2 st sy)

^{1}H NMR (300 MHz DMSO-d_6) δ: 9.2 (phenolic -OH), 8.4 (aromatic, near to NO_2), 8.1(4H aromatic, near to -N=N-), 7.8 (aromatic hydrogen from ester amide near to -CO), 7.5 (aromatic hydrogen from ester amide near to -N=N-), 7.3 (amino acid phenyl ring near to -N=N-), 7.1 (amino acid phenyl ring near to $-CH_2$), 6.7 (amino acid phenyl ring near to -OH), 5.1 (s, 2H, $-CH_2$ of BHDM), 4.8(-CH), 4.2, 4.3 ($-CH_2$)

Pol-V.5

Yield: 72%

Spectral properties

UVλ_{max} (solid): 280 (biphenyl), 362 ($\pi \rightarrow \pi^*$, N=N), 323 ($n \rightarrow \pi^*$, NO_2)

IR(KBr pellet) cm^{-1} : 3393 (NH st, OH st), 1730 (aromatic ester carbonyl), 1685 (amide I carbonyl stretch), 1530 (NO_2 st as, amide II st sy), 1423 (-N=N- st), 1349 (NO_2 st sy), 900-750 (ar CH)

^{1}H NMR (300 MHz DMSO-d_6): δ 9.2 (phenolic -OH), 8.4 (aromatic, near to NO_2), 8.1(4H aromatic, near to -N=N-), 7.8 (aromatic hydrogen from ester amide near to -CO), 7.5 (aromatic hydrogen from ester amide near to -N=N-),7.4 (aromatic, biphenyl) 7.3 (amino acid phenyl ring near to -N=N-), 7.1 (amino acid phenyl ring near to $-CH_2$), 6.7 (amino acid phenyl ring near to -OH), 6.5 (aromatic, biphenyl), 4.8(-CH), 4.2, 4.3 ($-CH_2$).

Pol-V-6

Yield: 73%

Spectral properties

UVλ_{max} (solid): 362 ($\pi \rightarrow \pi^*$, N=N), 323 ($n \rightarrow \pi^*$, NO_2)

IR(KBr pellet) cm^{-1} : 3393 (NH st, OH st), 1730 (aromatic ester carbonyl), 1685 (amide I carbonyl stretch), 1530 (NO_2 st as, amide II st sy), 1423 (-N=N- st), 1349 (NO_2 st sy), 800-760 (characteristic of naphthalene)

^{1}H NMR (300 MHz DMSO-d_6): δ 9.2 (phenolic -OH), 8.4 (aromatic, near to NO_2), 8.1(4H aromatic, near to -N=N-), 7.8 (aromatic hydrogen from ester amide near to -CO), 7.5 (aromatic hydrogen from ester amide near to -N=N-),7.1, 7.2 (aromatic, naphthalene 7.3 (amino acid phenyl ring near to -N=N-), 7.1 (amino acid phenyl ring near to $-CH_2$),6.9 (aromatic, naphthalene), 6.7 (amino acid phenyl ring near to -OH), 4.8(-CH), 4.2, 4.3 (CH_2)

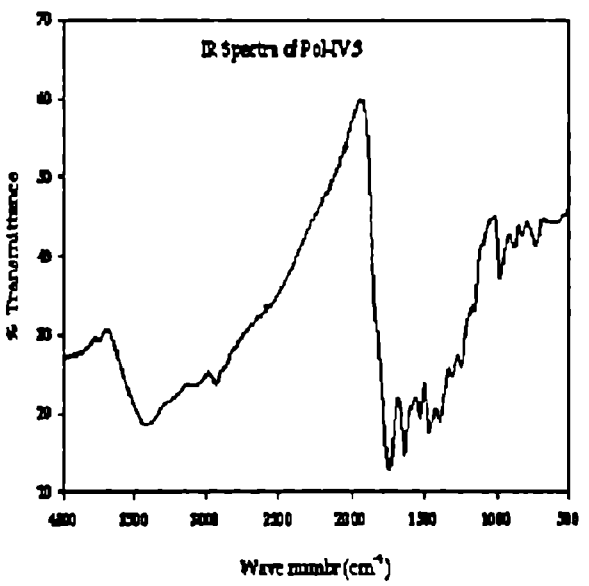

Figure. 5.14 IR spectrum of Pol-V.3

IR spectrum of polymers (**Figure. 5.14**) has shown two distinct carbonyl peaks at 1730-1715cm^{-1} and 1680-1700 cm^{-1}. These peaks can be attributed due to aromatic ester carbonyl and due to amide linkage. In the amide linkage, -CO is directly connected to -NH. This decreases the frequency of C=O str. to a lower value than the ester carbonyl. Presence of two distinct carbonyl peaks has confirmed the esterification of TYAZCl with the different diols.

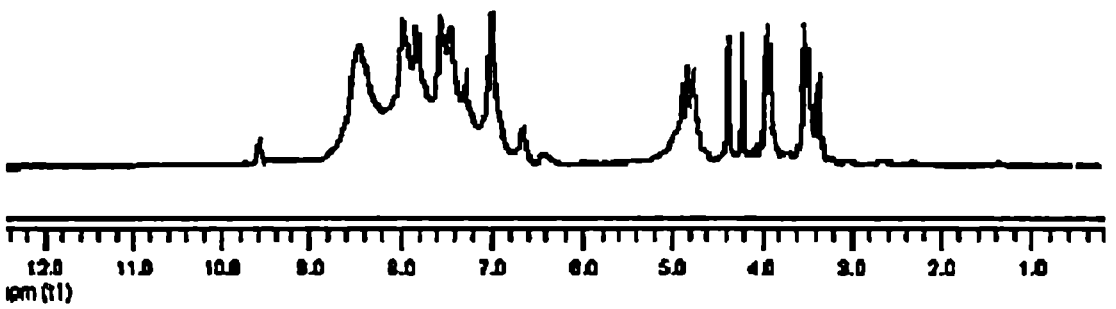

Figure 5.15. ^{1}H NMR spectrum of **Pol-V.3**

The multiplet at δ 4.3 in ^{1}H NMR spectrum (**Figure 5.15**) of TYAZCl has moved towards δ 4.8 in all polymers, which confirms the esterification. The hydrogens near Cl are more shielded (higher electron density) than the hydrogens near oxygen. So H connected to Cl has appeared at higher field. In **Pol-V-1** the aromatic region contains seven distinct peaks in the aromatic region and peaks at lower aliphatic region δ 3.1, δ 2.4, δ 2.1, δ 1.24 which confirmed the presence of camphanediol. Also in Pol-**V.2** and **Pol-V.3** there are seven distinct peaks in the aromatic region and the lower aliphatic peaks at δ 4.2, 4.3δ, 4.0, δ 3.5, δ 3.3 which confirmed the presence of isosorbide and isomanide. **Pol-V. 4** have more than seven aromatic peaks and the singlet at δ 5.1 due to $-CH_2$ in BHDM confirmed the esterification of TYAZCl with BHDM. **Pol-V.5** and **Pol-V. 6** contain the aromatic peaks due to TYAZCl and the diols of biphenyl and naphthalene respectively.

Because of the low solubility of the high molecular weight polymers recording of ^{13}C NMR spectrum in solution was difficult. As representative spectrum, solid-state ^{13}C NMR of polymer **Pol-V.3** was taken. It is shown in **Figure 5.16**. Instead of separate peaks ^{13}CNMR spectrum exhibits broad bands in the aromatic and aliphatic regions. But two different kinds of carbonyl carbon at δ 244 and δ 197 confirmed the presence of ester formation of TYAZCl with the diol, isosorbide. The broad band ranging from δ 160 to δ 110 agrees with the aromatic region of the polymer. The band from δ 80 to δ 20 agrees with the aliphatic region of the polymer.

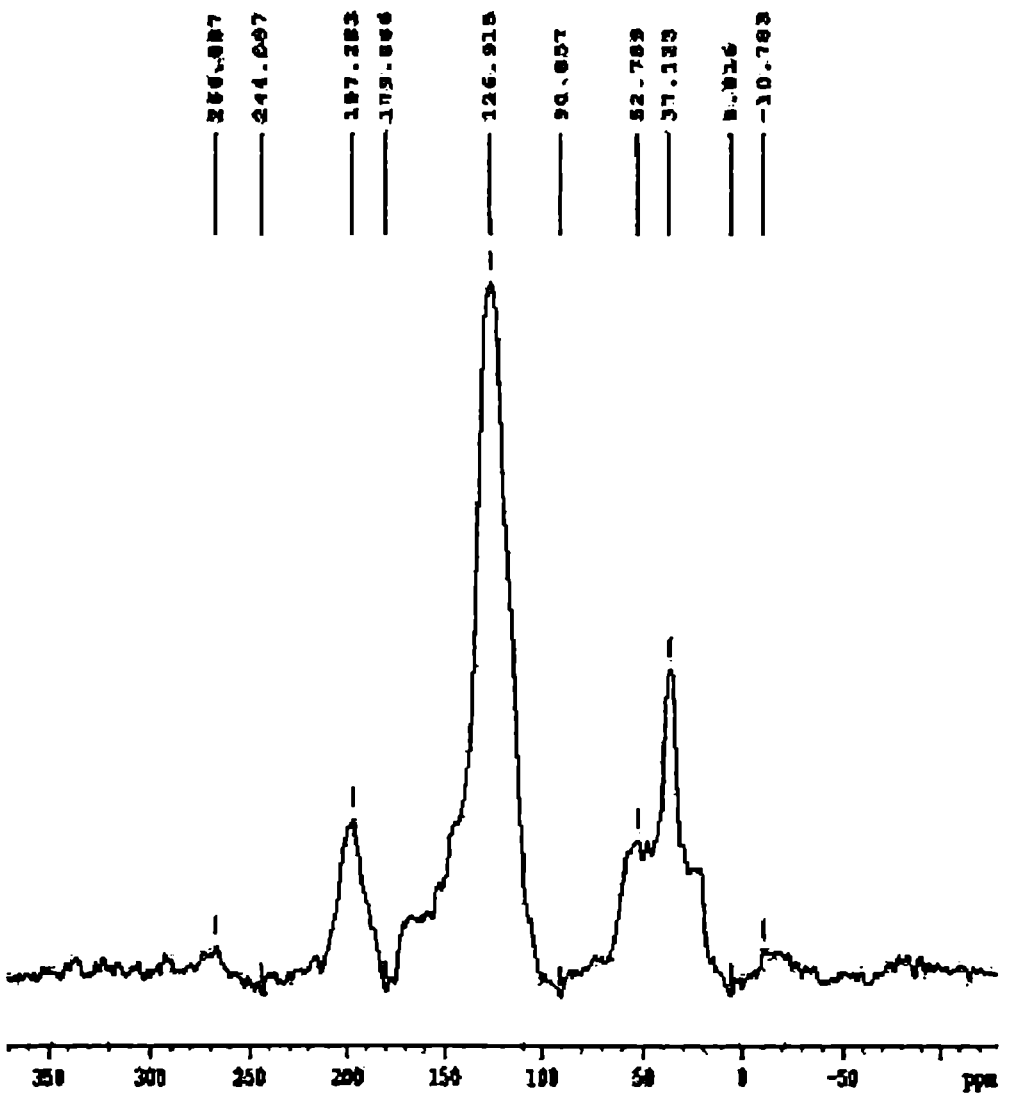

Figure 5.16. Solid State ^{13}C NMR spectrum of **Pol-V.3**

MALDI TOF Mass spectrum (**Figure 5.17**): The mass spectrum of **Pol-V.4** (m/e = 20340) gives an idea about the degree of polymerization. It showed that 15 monomeric units (one monomeric unit = 1356) were involved in the polymerization. The high temperature polycondensation method has yielded comparatively high molecular weight poly (ester -amide) s with a molecular weight up to twenty thousand

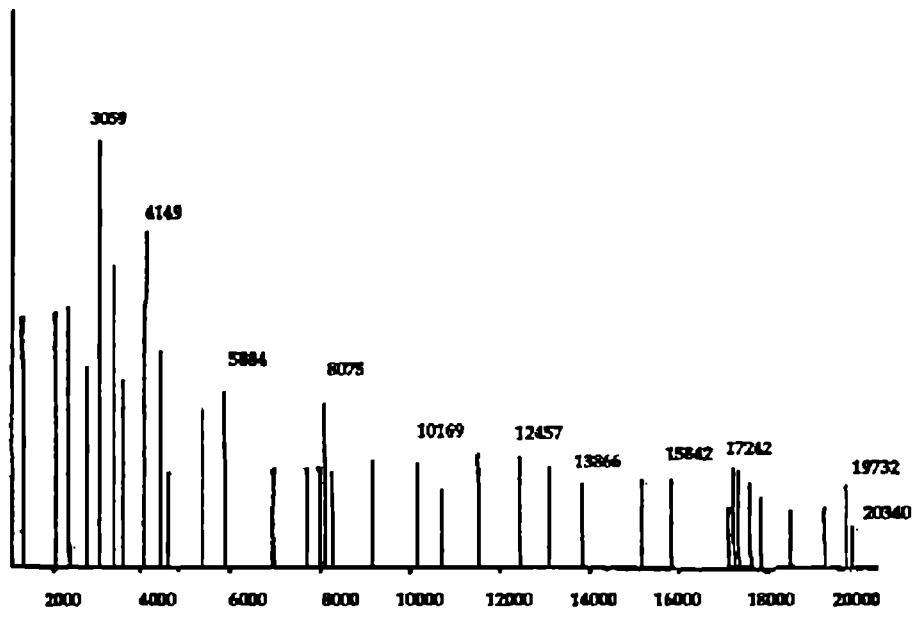

Figure 5.17 Mass spectrum of **Pol-V-4**

5.4.2.2. Thermal properties of the polymers

Since Tg and polar order in polymers are directly related, high value of Tg indicates high polar order. Tg values are shown in **Table.5.16**. The polymers with isomanide and camphanediol have high Tg values. This shows the polymer chains exhibit long range order which creates high degree of polar order in these polymers. Tg values reflect in the SHG efficiency. The one with higher Tg has given higher SHG efficiency. This may be explained based on the higher polar order of the polymers. In this series also the stereochemical effect and polar order are prominent. The polymer containing isosorbide has low value of Tg compared to the polymer containing its diastereomer, isomanide and this reflects the polar order in polymer containing isomanide. The low value of Tg for **Pol-V.5** may be attributed due the rotational behavior of the biphenyl ring (as a part of long polymer chain). This rotation gives flexibility to the -C-C- bond and gives a low value of Tg

The initial decomposition temperature (IDT) gives an idea about the thermal stability of the polymers. Except for the polymer having dihydroxy biphenyl all the poly

(ester-amide) s have IDT higher than 275^0 C. For the polymer with dihydroxy biphenyl it is 236^{0}C. From the Tg data it can be seen that all the polymers showed higher polar ordering with fairly good thermal stability.

5.5. Evaluation of second harmonic generation efficiency

The NLO efficiencies of poly(ester-amide) s were determined with 2-methyl-4-nitroaniline as the standard using Kurtz and Perry method.[18] Measurements were done by the powder method with a Quanta-Ray Nd-YAG laser from Spectra Physics (1064 nm, 10 ns,365mJ/S) integrated over 20 pulse and an average of 10 pulse. The samples were ground and graded with standard sieves to the phase matchable size (100-150 μm) and loaded on cuvette with 1mm thickness. MNA samples used as standards were also powdered and sieved (100-150 μm) after drying under high vacuum. They were also mounted with the same thickness as the polymer sample. The laser beam was directed unfocused onto the sample kept at a 45^0 angle to the laser beam which provides the phase comparable situation; the emission was collected from the front face of the sample at 90^0 angle. The SH signal; at 532 nm was detected by Avantes 2048 spectrometer with CCD camera. The results are shown in **Table 5. 16.**

Table 5.16: Yield and Properties of Poly(ester-amide) s

Polymer	Diol molecule	Yield (%)	*Tg* (*^{0}C*)	*IDT* (*^{0}C*)	$[\alpha]_D$	*SHG Efficiency**
Pol-V.1	Camphanediol	71	293.97	291	-24.3	8.53
Pol-V.2	Isosorbide	78	154.27	297	-23.2	7.73
Pol-V.3	Isomanide	75	299.43	287	-20.4	7.93
Pol-V.4	BHDM	74	215.67	275	-16.8	8.02
Pol-V.5	Dihydroxy bipehnyl	72	191.89	236	-18.0	7.60
Pol-V.6	Dihydroxy naphthalene	73	197.51	280	-15.9	7.54

*(SHG efficiency of MNA was taken as 1)

Table 5.16 gives the properties of the synthesized poly (ester-amide) s. All the poly (ester-amide) s are efficient materials for SHG with more than seven times SHG response compared to MNA. This is because of the helical structure of the poly (ester-amide) s due to the L-tyrosine based chiral framework. (**Figure 5.17.**). High NLO activity of the poly (ester-amide) s is because of highly extended chiral framework. The main consideration of this chapter was to achieve the chirality through the polymer chain rather than incorporating a chiral molecule as explained in chapter 4. This framework imparts the main chain chirality through out the entire chain, which induces chemical poling with out requirement for the external poling. The chiral framework significantly (up to eight times that of SHG of MNA) enhances the nonlinear optical susceptibility of the copolymers. The data for percentage chirality confirmed the extended chirality of the polymer chains to a long-range order. Since these polymers are oriented as a helix, it is assumed that the copolymers have broken symmetries along the substrate normal. They therefore, belong to the symmetry group C_∞; even though the monomeric units belong to C_1 point groups. For such samples with C_∞ symmetry, there are four nonvanishing macroscopic susceptibility components, that is χ_{zzz}, χ_{xxz} , χ_{zxx} and χ_{xyz}. The first three components originate from the polar ordering, while the latter can only be present in chiral media. Out of the four nonvanishing macroscopic susceptibility components, i.e χ_{zzz}, χ_{xxz} , χ_{zxx} and χ_{xyz}, the chiral susceptibility components χ_{xyz} is highly pronounced in this series of polymers due to two reasons: 1) the long range order of chiral frame work 2) the helical orientation of the poly(ester-amide) s (**Figure 5.18**). The long-range order of chiral framework

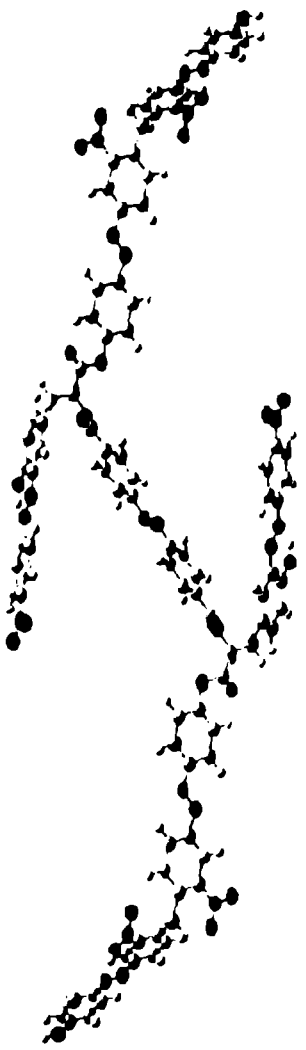

Figure 5.18 Helical structure of **Pol-V.4**

decreases the dipolar interactions. The Tg data proved that the polar order is also significantly high. These highly ordered structures of the polymers exist as a repeating unit of the chiral framework. This results the large nonchiral susceptibility component, χ_{zzz}, χ_{xxz} , χ_{zxx}. Strong coupling exists between the helical chiral framework and the diols, which resulted in a tightly packed highly ordered polymer framework ideal for high performance NLO active material. The electron delocalisation due to the π-π^* transition of the azobenzene system induces a displacement of electrons along the helical conjugated backbone. Here also, the stereochemical effect as explained and proved in chapter 4 plays its role. Out of the two-diastereomeric diols used for the polycondensation with the chiral framework, the poly (ester-amide) s with isomanide has high SHG value than the isosorbide poly (ester-amide) s. This is because of the more ordered structure, which reduces the dipolar interaction, of the isomanide based poly (ester-amide) s and which was proved from the. Tg results The polymer incorporated with BHDM showed SHG values more than the isosorbide, isomanide systems can be ascribed as the pronounced chiral contribution in the macroscopic level from the Λ helical nature of the poly (ester-amide) s inherited by the BHDM.

5.6. Correlation of theoretical and experimental results

The SHG efficiency has shown almost similar trends in theoretical calculation and experimental measurements (**Table 5.17**). Experimental measurements showed that all of the polymers have high SHG efficiency than MNA as predicted by theory. Polymers with camphanediol have the maximum susceptibility values in both theoretical calculation and also by experimental measurement. In agreement with the theory, the effect due to incorporation of chiral diol is not prominent in experimental measurements also. In experimental measurement, the least value is for binaphthalene system (**Pol-V.6**). By both theoretical calculation and experimental measurement, the less efficient one is isosorbide system (**Pol-V.2**). This may be due to the more scattering tendency of the binaphthalene system occurred during the experimental measurements or higher-level contribution will be more in isosorbide and thus the failure of 82 level ZINDO SOS calculation and derivative level CPHF calculation.

Except for **Pol-V.6** the ZINDO SOS (dynamic) calculation is in good agreement with the experimental results. The variation in *static* calculation is because of the derivative formalism rather than the SOS one. In experimental measurements, electrons will go to possible higher energy states, thus higher energy contribution may not be too small to be neglected. But *ab initio*-CPHF is numerically more accurate and precise in predicting the trends with high-level electron correlation. This defect can be rectified by introducing more electron correlation in frequency dependent CPHF calculation (CPHF *dynamic*). These calculations are computationally high demanding and can be achieved only with supercomputers for the systems with more than 500 electrons.

Table 5.17: Comparison of theoretical calculation with experimental measurements

Polymer	$\beta(10^{-30})esu$ (Static)	$\beta(10^{-30})esu$ (Dynamic)	SHG Efficiency*
Pol-V.1	35.9861	2168.197	**8.53**
Pol-V.2	14.4112	762.805	7.73
Pol-V.3	18.8488	1536.880	7.93
Pol-V.4	26.9000	1797.502	8.02
Pol-V.5	33.6258	1966.639	7.60
Pol-V.6	34.7583	1466.959	7.54
MNA	5.2684	198.9601	**1.00**

*Experimental values of polymers compared with that of MNA

5.7. Conclusion

A series of poly (ester-amide) s based of L-tyrosine chiral framework was designed and the properties were predicted. The goal of obtaining chirality along with the framework was achieved by this design. Theoretical calculation showed that all the polymers were highly efficient NLO materials. Synthesis of these poly (ester-amide) s in high yields could also be achieved. Experimental measurements of SHG were in good agreement with theoretical predictions as all the polymers have shown high SHG efficiency compared to MNA.

References

(1) Chemla, D. S.; Zyss, J. *Nonlinear Optical Properties of Organic Molecules and Crystals*; Academic Press, Inc: Newyork, **1987**

(2) Monaco, S. B.; Davis, L. E.; Velsko, . S. P.; Wang F. T.; Eimerl D.; Zalkin A. *J. Cryst. Growth* **1987**, *85*, 252)

(3) Ranganathan, D.; Kurur, S.; Madhusudanan, K. P.; Karle, I. L. *Tet. Lett.* **1997**, *38*, 4659

(4) Razzetti, C.; Ardoino, M.; Zanotti, L.; Zha, M.; Paorici, C. *Cryst. Res. Technol.* **2002**, *37*, 456.

(5) Kumar, G. R.; Raj, G. S.; Sankar, R.; Mohan, R.; Pandi, S.; Jayavel, R. *J. Cryst. Growth* **2004**, *267*, 213

(6) a) Yu, L. P.; Chan, W.; Bao, Z. *Macromolecules* **1992** *25*, 5609. (b) Stenger-Smith, J. D.; Henry, R. A.; Hoover, J. M.; Lindsay, G. A.; Nadler, M. P.; Nissan, R. A. *J. Polym. Sci., Part A: Polym. Chem.* **1993**, *31*, 2899. (c) Weder, C.; Neuenschwander, P.; Suter, U. W.; Pre´tre, P.; Kaatz, P.; Gu¨nter, P. *Macromolecules* **1995**, *28*, 2377

(7) Philip, B. *Studies on Photorestructuring of Synthetic Polymers* PhD thesis, University of Kerala, **2001**

(8) (a) Eckl, M.; Mu¨ller, H.; Stroriegl, P. *Macromol. Chem. Phys.* **1995**, *196*, 315. (b) Chern, Y.-T. *J. Polym. Sci., Part A: Polym. Chem.* **1996**, *34*, 133 (c) Akiyama, E.; Ohtomo, M.;Nagase, Y.; Koide, N. *Macromol. Chem. Phys.* **1995**, *196*, 3391.)

(9) (a) Hohenberg, P.; Kohn, W. *Phys. Rev.* **1964**, *136*, B864. (b) Kohn, W.; Sham , L. J. *Phys. Rev.* **1965**, *140*, A1133. (c) Salahub, D. R.; Zerner, M. C. *The Challenge of d and f Electrons*; ACS: Washington, D.C., **1989**). (d) Parr, R. G.; Yang, W. *Density-Functional Theory of Atoms and Molecules*; Oxford Unv. Press: Oxford, 1989.

(10) Gerratt , J.; Mills, I. M. *J. Chem. Phys.* **1968**, *49*, 1719 .

(11) Ridley, J.; Zerner, M. C. *Theor. Chim. Acta* **1973**, *32*, 111. Bacon, D.; Zerner, M. C. *Theor. Chim. Acta* **1979**, *53*, 21.

(12) Dewar, M. J. S.; Zoebisch, E. G.; Healy, E. F.; Stewart, J. J. P *J. Am.Chem. Soc.* **1985**, *107*, 3902.

(13) Levin, B. F. *Chem. Phys. Lett.*, **1976**, *37*, 516.

(14) Eliel, E. L.; Wilen, S. H. *Stereochemistry of Organic Compounds*; Wiley: New York, 1994

(15) (a) Vogel, A. I.A *Text Book of Practical Organic Chemistry*; Longman group: London, 1973 (b) Kalsi, P. S. *Organic Reactions and their Mechanisms;* New Age International: New Delhi, **2000**

(16) Pretsch, E.; Buhlmann, P; Affolter, C; *Structure Determination of Organic Compounds Tables of spectral Data*; Springer: Tokyo, 2000.

(17) Jakubke, H.D.; Jeschkeit, H *Amino acids, peptides and proteins*: Akademic press: Berline, **1977**

(18) Kurtz, S. K.; Perry, T. T. *J. Appl. Phys.* **1968**, *39*, 3798